Int J Comput Vis (2009) 82: 264–283
DOI 10.1007/s11263-008-0199-4

Four-Color Theorem and Level Set Methods for Watershed Segmentation

Erlend Hodneland · Xue-Cheng Tai · Hans-Hermann Gerdes

Received: 8 November 2007 / Accepted: 18 November 2008 / Published online: 17 December 2008

Abstract A marker-controlled and regularized watershed segmentation is proposed for cell segmentation. Only a few previous studies address the task of regularizing the obtained watershed lines from the traditional marker-controlled watershed segmentation. In the present formulation, the topographical distance function is applied in a level set formulation to perform the segmentation, and the regularization is easily accomplished by regularizing the level set functions. Based on the well-known Four-Color theorem, a mathematical model is developed for the proposed ideas. With this model, it is possible to segment any 2D image with arbitrary number of phases with as few as one or two level set functions. The algorithm has been tested on real 2D fluorescence microscopy images displaying rat cancer cells, and the algorithm has also been compared to a standard watershed segmentation as it is implemented in MATLAB. For a fixed set of markers and a set of challenging images, the comparison of these two methods shows that the present level set formulation performs better than a standard watershed segmentation.

Keywords Watershed · Level set · Four-Color theorem · Cell segmentation · Markers

The authors wish to thank Steffen Gurke and Nickolay Bukhoresthliev for providing the majority of pictures in this work. Erlend Hodneland was supported by the Norwegian Cancer Society, project number A05103/004.

E. Hodneland · H.-H. Gerdes
Department of Biomedicine, University of Bergen,
Jonas Lies vei 91, 5009 Bergen, Norway

X.-C. Tai (✉)
Division of Mathematical Sciences, School of Physical and Mathematical Sciences, Nanyang Technological University,
Singapore 637616, Singapore
e-mail: xctai@ntu.edu.sg

X.-C. Tai
Department of Mathematics, University of Bergen,
Johannes Brunsgate 12, 5007 Bergen, Norway
e-mail: tai@mi.uib.no

1 Introduction

Segmentation is a major challenge in image analysis, referring to the task of detecting boundaries of objects of interest in an image. Several approaches have been proposed. Two important classes of segmentation approaches are the so-called energy-driven segmentation (Caselles et al. 1993; Nielsen et al. 2006; Christiansen et al. 2006; Lie et al. 2005, 2006a; Vese and Chan 2002; Cremers et al. 2002; Kass et al. 1988) and watershed-based (Najman and Schmitt 1994; Meyer 1994; Vincent and Dougherty 1994; Vincent and Soille 1991). Energy-driven segmentation normally uses an energy functional consisting of two parts, i.e. a data term and a regularizer. The data term assures a solution which is sufficiently close to the desired boundaries and the regularizer controls the smoothness of the obtained contours. A smoothing is often required due to noise and artifacts in real images. Watershed segmentation (Najman and Schmitt 1994; Meyer 1994; Vincent and Dougherty 1994; Vincent and Soille 1991) is a region growing technique belonging to the class of morphological operations. Traditionally, the watershed techniques have been conducted without a smoothing term, but recent progress has resulted in energy-based watershed segmentations that contain regularizers. In the following the energy-driven and the watershed based segmentation approaches are described more carefully.

The energy-driven segmentation methods are mainly divided into two classes, contour-based (snakes) and region-based. The contour based methods rely on strong edges or ridges as a stopping term in a curve evolution which is balanced between a data term and a smoothness term. The snake approach has been studied in Kass et al. (1988), Caselles et al. (1993). Cremers et al. (2002) included statistical shape knowledge to the Mumford-Shah functional and Xu and Prince (1998) introduced the gradient vector flow (GVF) incorporating a global and external force which improved the capture range of their parametrical snake. One of the most well-known region-based methods is the Mumford and Shah (1989) model. In Vese and Chan (2002), Chan and Vese (2001), the Osher-Sethian level set idea (Osher and Sethian 1988) was combined with the Mumford-Shah model to solve the region-based segmentation. Recently, some variants of the Osher-Sethian level set idea was proposed by Tai et al. (Lie et al. 2005, 2006a, 2006b). A good survey of variational segmentation methods can be found in Chan et al. (2006).

The watershed segmentation has proven to be a powerful and fast technique for both contour detection and region-based segmentation. In principal, watershed segmentation depends on ridges to perform a proper segmentation. For region-based segmentation it is possible to convert the edges of the objects into ridges by calculating an edge map of the image. The watershed transform algorithms can be divided into two groups (Roerdink and Meijster 1999), either based on the recursive flooding algorithm of Vincent and Soille (1991), Rambabu and Chakrabarti (2007), Chien et al. (2003), Felkel et al. (2002), Najman and Schmitt (1994) or by different distance functions by Meyer (1994), Nguyen et al. (2003), Grau et al. (2004), Osma-Ruiz et al. (2007). The former can be understood as a landscape which is flooded recursively and the watershed lines appear where the water from two different basins meet. The latter is computed from variants of the topographical distance, which can be implemented as a priority queue. Among these, different watershed methods use slightly different distance measures, but they all share the property that the watershed lines appear as the points of equidistance between two adjacent minima. A common problem for the watershed transform is over-segmentation. However, watershed implemented by region growing based on a set of markers can avoid severe over-segmentation (Vincent and Soille 1991; Vincent and Dougherty 1994; Felkel et al. 2002). For the present work we use the topographical distance function as the method of choice, and we also create markers to reduce over-segmentation.

The success of a watershed segmentation depends on whether the desired boundaries are ridges. Unfortunately, the standard watershed framework has a very limited flexibility on optimization parameters, for example, there exists no possibility to smooth the boundaries. However, recent progress allows a regularization of the watershed lines (Nguyen et al. 2003) with an energy-based watershed algorithm (watersnakes). In contrast to the standard watershed and the watersnakes, our work is based on partial differential equations. This easily allows a regularization of the watershed lines. Moreover, the method is flexible with regard to additional optimization parameters, for instance the size of the watershed regions (Sect. 4.10) or the Euler number to avoid internal holes (not shown).

It seems that level set methods have never been used for watershed segmentation. In this work, we shall combine the traditional level set methods (Vese and Chan 2002) and the new variants (Lie et al. 2005, 2006a, 2006b) with watershed segmentation ideas. In Sect. 2, the foundation of our methods including the creation of the markers, the needed distance function and the Four-Color theorem are introduced. In Sect. 3, several level set methods are combined with the watershed segmentation idea using the topographical distance function. Combined with the Four-Color theorem, only one or two level set functions are needed to segment arbitrary numbers of regions (Vese and Chan 2002; Nath et al. 2006). Implementation and numerical details are supplied in Sect. 4. Experiments with real data are given to demonstrate the performance of the proposed algorithms compared to the traditional watershed methods. It is shown that the methods can identify arbitrary number of regions just with one level set function.

2 Introductory Steps

2.1 Active Contours and Cell Segmentation

A segmentation of the whole cell, the cell cytoplasm or any subcellular compartment can be obtained if a suitable fluorescent marker is available. A nucleus segmentation is an example of a segmentation of a subcellular compartment. Cytoplasmic (Bengtsson et al. 2004; Lindblad 2002; Adiga et al. 2006) or nucleus segmentation (Adiga and Chaudhuri 1999; Adiga 2003; Ortizde De Solorzano et al. 2001; Malpica et al. 1997; Wählby et al. 2004) was frequently reported in the past compared to whole cell segmentation which was poorly addressed (Ortizde De Solorzano et al. 2001; Baggett et al. 2005; Dow et al. 1996). It has the advantage compared to cytoplasmic segmentation that adjacent cells can be detected without merging them. Active contour models were used to detect neuronal axons (Fok et al. 1996), for nucleus segmentation (Bamford and Lovell 1998; Gebhard et al. 2001; Dufour et al. 2005) and whole cell segmentation (Ortizde De Solorzano et al. 2001). In the active contour model, each seed point (or marker region) gives rise to a closed contour (snake) evolving until conver-

gence. Then, the boundary of the cell should be captured. This process is repeated for all markers. However, boundary information between separate snakes from the different markers is mostly not connected to each other and therefore the resulting segmentation can result in regions of either vacuum or overlap. To deal with this problem, different conflict measures or restrictions of movement for the snakes to avoid overlap have to be implemented (Fok et al. 1996; Bamford and Lovell 1998). Our level set watershed, which shall be introduced in Sect. 3, is implicitly defined in such way that vacuum or overlap will never occur. This property is important in cell segmentation since cells are individual compartments, and the final segmentation should define every pixel either as part of one and only one cell, or as part of the background. Furthermore, a parametrical snake requires often one snake per object, or for the implicit snake, the number of level set functions is proportional to the number of objects as $\propto \log n$ when n is the number of objects or phases. Thus, the complexity increases swiftly for images containing a high number of cells. Due to the Four-Color theorem, c.f. Sect. 2.4, we are able to keep the number of level set functions at a very low level, independent of the number of objects to be segmented.

2.2 Creating Markers

Marker-controlled watershed segmentation is a robust and flexible method for segmentation of objects with closed contours where the boundaries are expressed as ridges. The marker image used for watershed segmentation is a binary image consisting of either single marker points or larger marker regions where each connected marker is placed inside an object of interest. Thus, each initial marker has a one-to-one relationship to the specific watershed region surrounded by the watershed lines. The final watershed segmentation is strictly depending on the markers, which is the case in the proposed watershed by level set, the watersnakes and the standard watershed. This dependency is a consequence of the one-to-one relationship as well as the size and position of the markers. Region-markers generally create results of higher quality than point-markers since their boundaries are closer to the desired boundaries and therefore there is a smaller probability of the flooding converging too early. The markers can be manually or automatically constructed, but high-throughput experiments often require automatically generated markers to save human time and resources. After segmentation, the boundaries of the watershed regions (watersheds) are arranged on the ridges, thus separating each object from its neighbors.

For the current project, the markers were automatically generated. The algorithm is sketched in the following and some detailed explanations are given afterward.

```
% ur: ridge enhanced raw image u
1. ur = ridge_enhancement(u)
% ua: after adaptive thresholding
2. ua = adaptive_thresholding(ur)
% ub: binary image after removal of small objects
3. ub = remove_small_objects(ua)
4. for i = 1 to (step = 1) 10
    a) se = get_structural_element(radius = i)
    b) closed = close(ub,se)
    c) filled = fill(closed)
    d) label = label_filled_regions(filled)
    % check for intersection of the filled areas to
    % previously filled areas
    e) for j = 1 to (step = 1) number_objects(label)
          if empty(intersection(object(j),markers))
          % this region has not been detected before and
          % is added to marker image
          markers(object(j)) = 1
% remove the smallest markers that normally
% represent an over–segmentation
5. markers = remove_small_objects(markers)
```

First, a Hessian ridge enhancement (Gautama et al. 2004) is applied to enhance the ridges of the raw image u (#1 in flowscheme). The ridges are of special interest since the cell boundaries appear as ridges. The ridge enhancement is based on the eigenvalue decomposition of a Gaussian smoothed Hessian matrix

$$H = G_{\sigma,\delta} \begin{pmatrix} u_{xx} & u_{xy} & u_{xz} \\ u_{yx} & u_{yy} & u_{yz} \\ u_{zx} & u_{zy} & u_{zz} \end{pmatrix}$$

where the parameters σ and δ are the standard deviation and the height of the filter in the Gaussian. The eigenvector corresponding to the largest eigenvalue λ_1 points along the ridge, and the other points perpendicular to the ridge. A ridge is characterized by $\lambda_1 < 0$ and $\lambda_2 \approx 0$ (Gautama et al. 2004), and is thus highlighted using a transfer function defined as $H(\lambda_1, \lambda_2) = -\lambda_1 - \lambda_2^2$, taking the highest values on the ridges. An example is given in Fig. 1 where the image (A) was used for Hessian ridge enhancement (B) ($\sigma = 2$ and $\delta = 5$). Clearly, the ridges are enhanced compared to other structures.

Adaptive thresholding (Chang et al. 2000; Gonzalez and Woods 1992) is used to automatically create binary marker regions from the ridge enhanced image (#2 in flowscheme). The adaptive thresholding has a much higher resistance against noise and inhomogeneous illumination than global thresholding for labeling of high intensity objects, in our case the ridges. The adaptive thresholding image u_a is computed as

$$u_a(x, y) = \begin{cases} 1 & \text{if } u_r(x, y) > \mu \max(u_r) + A_\delta(u_r, x, y), \\ 0 & \text{else,} \end{cases}$$

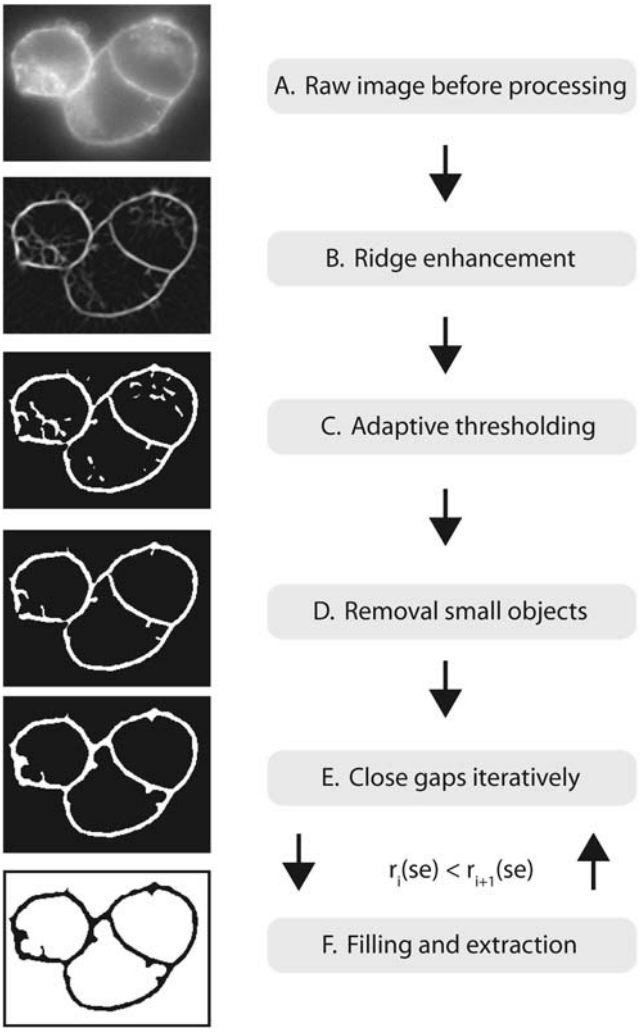

Fig. 1 Automated construction of markers. The image (**A**) is used for ridge enhancement (**B**) to improve the signal intensity of the ridges. An adaptive thresholding is applied to detect the ridges and convert them into binary structures (**C**). The smallest objects are removed due their size (**D**) and a morphological closing is performed to close gaps in the binary structure (**E**). The closing is repeated iteratively with increasing radius r of the circular structural element (se), $r_i(\text{se}) < r_{i+1}(\text{se})$. A binary filling is computed after the closing at each iterative step (**F**) and all binary objects of the size within a user-defined interval are selected and used as marker regions. However, the objects are only selected if they have no intersection to previously selected objects. This enables larger marker regions with their boundaries closer to the true boundaries of the desired objects

where μ is a user-defined scalar threshold with typical values of $[0.01 \rightarrow 0.2]$ and δ is the filter dimension of the average filter A_δ. $A_\delta(u_r, x, y)$ is the average values of u_r in a δ-neighborhood of (x, y). The image in Fig. 1(C) is an example of the adaptive thresholding with $\delta = 20$ and $\mu = 0.06$. All small objects in u_a are removed since they are considered to be insignificant due to their size (D in Fig. 1, #3 in the flowscheme). To be able to close minor gaps in the binary structures outlining the approximate boundaries, an iterative morphological closing is conducted (E in Fig. 1, #4 in the flowscheme). For each iterative closing step, a larger structural element is applied to facilitate the closing of incrementally larger gaps. Directly after every closing step, each filled region is labeled uniquely (#4d in flowscheme) and morphological filling is used to detect all holes in u_b that were not accessed from the image boundary (#4e in the flowscheme). All regions with a size within an interval and with no intersection to earlier filled regions are assigned to the marker image as a marker (F in Fig. 1, #4e in the flowscheme). The closing is repeated iteratively with increasing radius r of the circular structural element (se), $r_i(\text{se}) < r_{i+1}(\text{se})$. This process is performed iteratively a predefined number of steps in order to obtain markers with boundaries as close as possible to the desired cell boundaries. Finally, removal of the smallest markers is necessary, using a threshold proportional to an estimated cell size (#5 in the flowscheme) which is a global setting normally remaining unchanged within the same cell line. Thus, within such experiments, the method is parameter free. High-throughput experiments normally allow a global setting of the estimated cell size, and the marker generation is therefore of great significance in such experiments including a large number of images. The automated marker generation has thoroughly been applied to large amount of data and an overall high marker quality was obtained (statistics not shown).

Note that a marker-controlled watershed segmentation is often preferred instead of a direct watershed segmentation which easily produces a serious over-segmentation due to the large number of natural minima in images. Every marker will have a one-to-one relationship to a watershed region and the major segmentation pattern is therefore already decided when the marker image is given. Thus, the standard marker-controlled watershed, the watersnakes and the watershed level set are all strictly depending on the markers, and the algorithms are limited to detecting the desired ridge in a closed contour around each marker.

2.3 Topographical Distance Function

We shall use the topographical distance function (Meyer 1994; Nguyen et al. 2003; Roerdink and Meijster 1999), closely related to the framework of minima paths (Arbeléz and Cohen 2004), for our watershed segmentation. In addition, level set methods will be incorporated into this segmentation framework. The topographical distance function between two points $\mathbf{x}$ and $\mathbf{y}$ is defined as (Nguyen et al. 2003; Roerdink and Meijster 1999):

$$L(\mathbf{x}, \mathbf{y}) = \inf_{\gamma \in [\mathbf{x} \rightarrow \mathbf{y}]} \int_\gamma |\nabla u(\gamma(s))| ds. \tag{1}$$

In addition, we define $L_i(\mathbf{x}) = \inf_{\mathbf{y} \in M_i} L(\mathbf{x}, \mathbf{y})$. Therefore $\exists \mathbf{y}_i^* \in M_i$ such that $L_i(\mathbf{x}) = L(\mathbf{x}, \mathbf{y}_i^*)$. Furthermore, let K be

the number of markers and let $\alpha_i = u(\mathbf{y}_i^*)$. Using $L_i(x)$, the definition of the *catchment basin* $CB(M_i)$ is given as below:

$$CB(M_i) = \{\mathbf{x} \in \Omega \mid \forall j \neq i, 1 \leq j \leq K : \alpha_i + L_i(\mathbf{x}) < \alpha_j + L_j(\mathbf{x})\}. \quad (2)$$

The parameter α_i works as a scaling of each minima to enable a comparison of the topographical distance functions between different minima. The watershed lines $W(u)$ are defined as the set of all points not belonging to any catchment basin. As $L_i(\mathbf{x})$ is continuous, $W(u)$ is equivalent to the points where $\alpha_i + L_i(\mathbf{x}) = \alpha_j + L_j(\mathbf{x}),\ i \neq j,\ i, j = \{1, \ldots, K\}$.

In the discrete case, the topographical distance function along the path $\pi = (p_0, \ldots, p_l)$ can be defined as (Roerdink and Meijster 1999)

$$L(p_0, p_l) = \min_{\pi \in [p \to q]} \sum_{i=0}^{l-1} d(p, q) cost(p_i, p_{i+1}), \quad (3)$$

which is the minimum value of all possible paths from p_0 to p_l. The cost for walking from pixel p to pixel q is related to the *lower slope* which is defined as the maximum slope linking p to any of its neighbors of lower altitude, $LS(p) = \max_{q \in N(p) \cup p} \frac{u(p)-u(q)}{d(p,q)}$. $N(p)$ is the set of neighbors around p and $d(p, q)$ is the distance between p and q. The cost for walking from any pixel p to a neighbour pixel q is given as

$$cost(p, q) = \begin{cases} LS(p) & \text{if } u(p) > u(q), \\ LS(q) & \text{if } u(q) > u(p), \\ \frac{1}{2}(LS(p) + LS(q)) & \text{if } u(p) = u(q). \end{cases} \quad (4)$$

In 1D the topographical distance function is straightforward to compute since there is only one possible path between any two points $\mathbf{x}$ and $\mathbf{y}$. For the present study, we have used the iterative forest transform (IFT) (Felkel et al. 2002; Roerdink and Meijster 1999) to compute the topographical distance function between a marker and any other point in the image.

2.4 Four-Color Theorem

We shall use the Four-Color theorem in our watershed segmentation combined with level set methods. The Four-Color theorem was proven first by Appel and Haken in 1976 (Appel and Haken 1977), and it has been validated again by different approaches in recent years (Robertson et al. 1996). Consider a set of regions (or countries) and select an arbitrary point inside each region (a capital). Join the points of every pair of neighboring regions with a line. Then, one arrives at the definition of a planar *graph*. The Four-Color theorem, c.f. Appel and Haken (1977), states that it is possible to label any 2D planar graph with as few as four colors such that no neighbors have the same color. Therefore, we could associate each watershed region with a color and use no more than four colors to mark the watershed regions. By doing so, adjacent objects can be labeled among four colors and they are thus uniquely distinguishable since any two neighboring watershed regions will be labeled with different colors. Using the Four-Color theorem it is therefore possible to segment an arbitrary number of objects with as few as four phases. Vese and Chan (2002) noted that the Four-Color theorem can be used in image segmentation in the piecewise smooth case to distinguish between any number of objects with as few as four phases. The Four-Color theorem was previously used for region based segmentation of stained cell nuclei using the Chan-Vese model (Nath et al. 2006). They reduce the number of level set functions significantly by grouping the objects into four colors. However, their approach is a region-based segmentation technique and not contour-based like the watershed level set.

2.5 Euclidean Influence Zones

The Four-Color coding must be applied to a planar graph with no vacuum between the regions. Therefore, it can not be applied directly to the markers which are objects with gaps in between. To overcome this problem, an approximation of the final object partition based on the markers is computed. Ideally, this partition should capture information about the final boundaries of the objects, reflecting the assumed neighborship between the regions. To obtain the approximation of the final boundaries, the Euclidean distance transform around each marker is computed. Larger marker regions provide a better approximation of the boundaries since the outer periphery of the markers is closer to the true object boundaries. Every pixel in the image is assigned to one influence zone of a marker such that each point from this zone has the smaller distance to this marker than to any other marker.

Mathematically, consider K markers and label all markers $\{M_i\}_{i=1}^K$. The Euclidean distance function $dist(\mathbf{x}, M_i)$ is calculated around each marker M_i. The Euclidean influence zone image f_{IZ} is a function defined as:

$$f_{IZ}(\mathbf{x}) = \{i \mid dist(\mathbf{x}, M_i) \leq dist(\mathbf{x}, M_j), \forall j = 1, \ldots, K\}. \quad (5)$$

Thus, $f_{IZ} = i$ if x has the shortest distance to marker M_i. So, f_{IZ} is a piecewise constant function taking values from 1 to K and the region where $f_{IZ}(x) = i$ is called the Euclidean influence zone of marker M_i. Figure 2 is an example of the Euclidean influence zones f_{IZ}. The image (a) was used to create markers automatically (b, see Sect. 2.2). The Euclidean influence zones (c) were obtained using (5). Thus, a piecewise constant image f_{IZ} is constructed where each

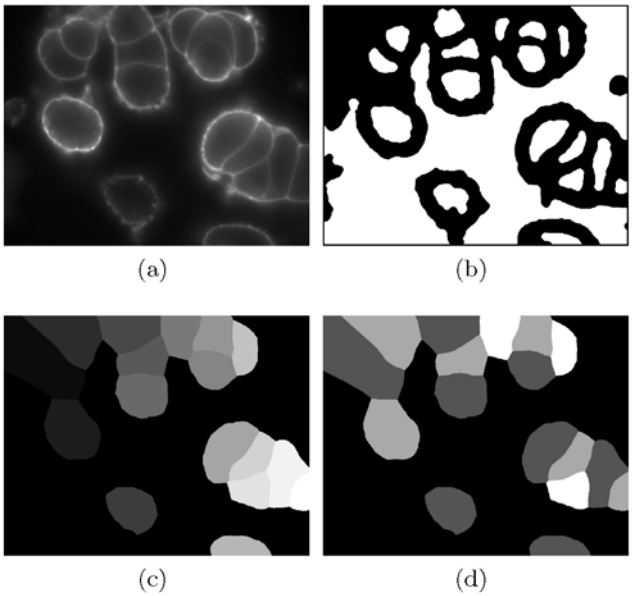

Fig. 2 Euclidean influence zones and the Four-Color theorem. The image in (**a**) was used to automatically create markers (**b**) using the method described in Sect. 2.2. The Euclidean influence zones f_{IZ} were computed around the markers, shown in (**c**) where each region is labeled by a unique integer value. The Four-Color theorem was applied to (**c**), resulting in (**d**) where no neighboring regions have the same color (*black*: 1, *dark grey*: 2, *light grey*: 3, *white*: 4)

region is uniquely labeled by an integer from $\{1, 2, \ldots, K\}$. These zones are suitable for a color coding using the Four-Color theorem. Figure 2d shows one possible Four-Color coding of (c), where no region has a neighbor with the same integer value.

3 Level Set Methods for Watershed Segmentation

After applying the Four-Color theorem to the Euclidean influence zones $f_{IZ} = i$, we get an approximation to the final boundaries for the segmentation. For the images in this paper, the painting of the regions was done by an automated code where various combinations were tried and faulty ones eliminated to achieve a true partition according to the Four-Color theorem. Thus, a final coloring $f_c(x) \in \{1, 2, 3, 4\}$ was obtained where adjacent influence zones and their corresponding markers are always assigned different colors, see an example of this in Fig. 2d. Empty colors will not influence the performance of the algorithm.

Once each marker has been painted with one of the four colors, the markers can be grouped into four groups, i.e., we define the group of markers $C_i = \bigcup_{f_c(M_j)=i} M_j$ and the boundaries of these, ∂C_i, $i = 1, 2, 3, 4$. The method of (Felkel et al. 2002) is then used to compute up to four topographical distance functions from each of the marker groups C_i, i.e., $L_i(\mathbf{x}) = \inf_{\mathbf{y}\in C_i} L(\mathbf{x}, \mathbf{y})$, $i = 1, 2, 3, 4$. It is true that there exists a $\mathbf{y}_i^* \in \partial C_i$ such that $L_i(x) = L(x, \mathbf{y}_i^*)$. Correspondingly, we also take $\alpha_i = u(\mathbf{y}_i^*)$. As was proven in (Tai et al. 2007), a partition $\{\Omega_i\}_{i=1}^4$ minimizes the functional

$$E(\Omega_1, \ldots, \Omega_4) = \sum_{i=1}^{4} \int_{\Omega_i} \{\alpha_i + L_i(\mathbf{x})\} d\mathbf{x} \tag{6}$$

if and if it is a watershed segmentation around the group markers defined by the four colors. The proof is essentially the same as given in Nguyen et al. (2003).

In the following, we propose to use level set methods to solve the above watershed segmentation problem. We shall use three different variants of the level set idea to accomplish the watershed segmentation based on the function $L_i, i = 1, 2, 3, 4$. These are the Chan-Vese level set (Chan and Vese 2001), the Binary level set (Nielsen et al. 2006) and a variant of the Piecewise constant level set (PCLS) (Lie et al. 2005, 2006b). In Tai et al. (2007) a short version of the watershed level set was described. In the current work, a new approach for the piecewise constant level set is presented. Moreover, further details for implementation are given and substantially more numerical examples are shown. Also, the watershed level set has been compared to the watersnakes.

3.1 Watersheds and the Chan-Vese Model

First, we propose to use the level set idea (Osher and Sethian 1988) as in Chan and Vese (2001, 2002) for the segmentation. Let $\phi_1(\mathbf{x}), \phi_2(\mathbf{x}) : \mathbb{R}^2 \to \mathbb{R}$ be two continuous level set functions defined on the domain Ω. Normally, ϕ_1, ϕ_2 are required to be distance functions to some curves, but this is not needed for our method here. These functions will partition the domain into four (possibly disconnected) sub-regions. The characteristic functions for these sub-regions are $\psi_i, i = \{1, 2, 3, 4\}$ given as

$$\psi_1(\phi_1, \phi_2) = H(\phi_1)H(\phi_2),$$
$$\psi_2(\phi_1, \phi_2) = (1 - H(\phi_1))H(\phi_2),$$
$$\psi_3(\phi_1, \phi_2) = H(\phi_1)(1 - H(\phi_2)),$$
$$\psi_4(\phi_1, \phi_2) = (1 - H(\phi_1))(1 - H(\phi_2)).$$

The sub-regions are $\Omega_i = \{\mathbf{x}|\ \psi_i(\mathbf{x}) = 1\}, i = 1, 2, 3, 4$. This partition of the domain has no vacuum and no overlaps. In the above, $H(\cdot)$ denotes the Heaviside function, i.e. $H(x) = 1$ if $x \geq 0$, $H(x) = 0$ if $x < 0$. For the numerical experiments, a regularized Heaviside was used, i.e., $H_\epsilon(x) = \frac{1}{2}(1 + \frac{2}{\pi}\arctan(\frac{x}{\epsilon}))$ where $\epsilon > 0$ is small, see Chan and Vese (2001). The relation $H'(x) = \delta(x)$ was used for differentiation of ψ_i, and a smooth $\delta_\epsilon(x)$ was used in the numerical experiments by calculating the derivative of the smooth Heaviside.

Assume that the sub-regions $\Omega_i, i = 1, 2, 3, 4$ are related to $\phi_i, i = 1, 2$ as above, then we see that

$$\sum_{i=1}^{4} \int_{\Omega_i} \{\alpha_i + L_i(\mathbf{x})\} d\mathbf{x} = \int_{\Omega} \sum_{i=1}^{4} \{\alpha_i + L_i(\mathbf{x})\} \psi_i(\phi_1, \phi_2) d\mathbf{x}. \tag{7}$$

Based on this observation, we can try to solve the following minimization problem:

$$\min_{\phi_1, \phi_2} \int_{\Omega} \sum_{i=1}^{4} \{\alpha_i + L_i(\mathbf{x})\} \psi_i d\mathbf{x}. \tag{8}$$

If $\{\phi_i\}_{i=1}^2$ is a minimizer of the above problem, then the corresponding sub-regions $\{\Omega_i\}_{i=1}^4$ is a watershed segmentation. In order to regularize the boundaries of the watershed regions, we shall add a regularization term into the minimization functional. Instead of solving (8), we try to minimize

$$\min_{\phi_1, \phi_2} F(\phi_1, \phi_2),$$
$$F = \int_{\Omega} \sum_{i=1}^{4} \{\alpha_i + L_i(\mathbf{x})\} \psi_i d\mathbf{x} + \lambda \int_{\Omega} \sum_{i=1}^{4} |\nabla \psi_i| d\mathbf{x}. \tag{9}$$

The first term is the data term providing the watershed segmentation and the second term is the regularization to ensure a sufficiently smooth boundary for the watershed segmentation. The regularization is performed on $\{\psi_i\}_{i=1}^4$ which is different from Chan and Vese (2001) where the regularization is performed directly on $\{\phi_i\}_{i=1}^2$. The difference between these two approaches is discussed in more details in Sect. 4.7. As described in Tai and Chan (2004), a minimization of (9) with regard to ϕ_1 and ϕ_2 produces the following Euler-Lagrange equations

$$\begin{aligned} \sum_{i=1}^{4} \frac{\partial \psi_i}{\partial \phi_1} \left(\alpha_i + L_i(\mathbf{x}) - \lambda \nabla \cdot \left(\frac{\nabla \psi_i}{|\nabla \psi_i|} \right) \right) = 0, \\ \sum_{i=1}^{4} \frac{\partial \psi_i}{\partial \phi_2} \left(\alpha_i + L_i(\mathbf{x}) - \lambda \nabla \cdot \left(\frac{\nabla \psi_i}{|\nabla \psi_i|} \right) \right) = 0. \end{aligned} \tag{10}$$

In order to get the above results, we need to use the chain-rule as in Tai and Chan (2004, p. 29) and Chan and Tai (2004, p. 45). The terms $\frac{\partial \psi_i}{\partial \phi_1}$ and $\frac{\partial \psi_i}{\partial \phi_2}$ are calculated as

$$\begin{aligned} &\frac{\partial \psi_1}{\partial \phi_1} = \delta(\phi_1) H(\phi_2), \qquad \frac{\partial \psi_1}{\partial \phi_2} = H(\phi_1) \delta(\phi_2), \\ &\frac{\partial \psi_2}{\partial \phi_1} = -\delta(\phi_1) H(\phi_2), \qquad \frac{\partial \psi_2}{\partial \phi_2} = (1 - H(\phi_1)) \delta(\phi_2), \\ &\frac{\partial \psi_3}{\partial \phi_1} = \delta(\phi_1)(1 - H(\phi_2)), \qquad \frac{\partial \psi_3}{\partial \phi_2} = -H(\phi_1) \delta(\phi_2), \\ &\frac{\partial \psi_4}{\partial \phi_1} = -\delta(\phi_1)(1 - H(\phi_2)), \\ &\frac{\partial \psi_4}{\partial \phi_2} = -(1 - H(\phi_1)) \delta(\phi_2). \end{aligned} \tag{11}$$

In numerical simulations, δ and H are replaced by their smoothed counter parts δ_ϵ and H_ϵ respectively. As usual, we can use the gradient descent method to solve these equations. With some initial conditions for $\{\phi_i\}_{i=1}^2$, the gradient flow equations are:

$$\begin{aligned} \frac{\partial \phi_1}{\partial t} &= -\sum_{i=1}^{4} \frac{\partial \psi_i}{\partial \phi_1} \left(\alpha_i + L_i(\mathbf{x}) - \lambda \nabla \cdot \left(\frac{\nabla \psi_i}{|\nabla \psi_i|} \right) \right), \\ \frac{\partial \phi_2}{\partial t} &= -\sum_{i=1}^{4} \frac{\partial \psi_i}{\partial \phi_2} \left(\alpha_i + L_i(\mathbf{x}) - \lambda \nabla \cdot \left(\frac{\nabla \psi_i}{|\nabla \psi_i|} \right) \right). \end{aligned} \tag{12}$$

The following explicit scheme will be used in our numerical experiments. Note that faster methods can be used to solve these equations. For example, the AOS scheme proposed in Lu et al. (1992, 1991) and re-discoverted in Weickert et al. (1998) can be used for the equations (12) similarly as in Li and Tai (2007b). The dual algorithm of Chambolle (2004) can also be used to get fast algorithms. In addition, the graph-cut techniques (Darbon and Sigelle 2006) could also be a powerful tool for these equations. For simplicity, we have only tested on the following explicit scheme so far:

$$\begin{aligned} \frac{\phi_1^{n+1} - \phi_1^n}{\tau} &= -\sum_{i=1}^{4} \frac{\partial \psi_i^n}{\partial \phi_1^n} \left(\alpha_i + L_i(\mathbf{x}) - \lambda \sum_{i=1}^{4} \nabla \cdot \left(\frac{\nabla \psi_i^n}{|\nabla \psi_i^n|} \right) \right), \\ \frac{\phi_2^{n+1} - \phi_2^n}{\tau} &= -\sum_{i=1}^{4} \frac{\partial \psi_i^n}{\partial \phi_2^n} \left(\alpha_i + L_i(\mathbf{x}) - \lambda \sum_{i=1}^{4} \nabla \cdot \left(\frac{\nabla \psi_i^n}{|\nabla \psi_i^n|} \right) \right), \end{aligned} \tag{13}$$

where $\psi_i^n = \psi_i(\phi_1^n, \phi_2^n)$. This iteration is not the fastest algorithm. However, it often converges in less than 200 iterations for our experiments.

3.2 Watersheds and the Binary Level Set

The second level set method we propose to use is the so-called Binary level set (Lie et al. 2005, 2006a; Song and

Chan 2002). This method has been used for image segmentation and inverse problems in Nielsen et al. (2007), Tai and Yao (2006). For this method, we need to find two functions $\phi_1(\mathbf{x}), \phi_2(\mathbf{x}) : \mathbb{R}^2 \to \mathbb{R}$ satisfying $\phi_i(\mathbf{x})^2 = 1,\ i = 1, 2$. These functions can also partition Ω into four sub-regions with the characteristic functions given by

$$\psi_{i+1+2*j} = \frac{1}{4}\left(1 + (-1)^i \frac{\phi_1}{|\phi_1|}\right) \times \left(1 + (-1)^j \frac{\phi_2}{|\phi_2|}\right), \quad i, j = 0, 1.$$

The sub-regions associated with the characteristic functions $\psi_i, i = 1, 2, 3, 4$ have no overlaps and vacuum. This method is closely related to the Chan-Vese model using two level set functions creating four sub-regions. However, the signum function is used instead of the Heaviside function. In the numerical experiments, $\phi/|\phi|$ are replaced by $\phi/\sqrt{|\phi|^2 + \epsilon}$ with a small $\epsilon > 0$.

Similar to (9), we solve the following minimization problem:

$$\min_{\phi_1, \phi_2} F(\phi_1, \phi_2), \tag{14}$$

$$F = \int_\Omega \sum_{i=1}^{4} \{\alpha_i + L_i(\mathbf{x})\}\psi_i d\mathbf{x} + \lambda \int_\Omega \sum_{i=1}^{4} |\nabla \psi_i| d\mathbf{x} + \sigma \sum_{i=1}^{2} \int_\Omega (\phi_i^2 - 1)^2 d\mathbf{x}. \tag{15}$$

Once the minimizer is obtained, the corresponding characteristic functions will give us the watershed sub-regions. In the above, the constant $\sigma > 0$ is a penalization constant to enforce $\phi_i^2 = 1$ and λ is the regularization parameter which influences the smoothness of the watershed lines. Due to the special constructions of the characteristic functions ψ_i, we can choose any $\sigma > 0$ in the above minimization functional. We need to use a large σ if the characteristic functions ψ_i are replaced by $\psi_{i+1+2*j} = \frac{1}{4}(1 + (-1)^i\phi_1)(1 + (-1)^j\phi_2)$. The Euler-Lagrange equations for minimization of problem (15) with respect to ϕ_1 and ϕ_2 are:

$$\frac{\partial F}{\partial \phi_1} = \sum_{i=1}^{4} \frac{\partial \psi_i}{\partial \phi_1}\left(\alpha_i + L_i(\mathbf{x}) - \lambda \nabla \cdot \left(\frac{\nabla \psi_i}{|\nabla \psi_i|}\right)\right) + 4\sigma\phi_1(\phi_1^2 - 1) = 0, \tag{16}$$

$$\frac{\partial F}{\partial \phi_2} = \sum_{i=1}^{4} \frac{\partial \psi_i}{\partial \phi_2}\left(\alpha_i + L_i(\mathbf{x}) - \lambda \nabla \cdot \left(\frac{\nabla \psi_i}{|\nabla \psi_i|}\right)\right) + 4\sigma\phi_2(\phi_2^2 - 1) = 0. \tag{17}$$

Again, we use the following explicit scheme to solve the corresponding gradient flow equations:

$$\begin{aligned}
&\frac{\phi_1^{n+1} - \phi_1^n}{\tau} \\
&= -\sum_{i=1}^{4} \frac{\partial \psi_i^n}{\partial \phi_1^n}\left(\alpha_i + L_i(\mathbf{x}) - \lambda \nabla \cdot \left(\frac{\nabla \psi_i^n}{|\nabla \psi_i^n|}\right)\right) \\
&\quad + 4\sigma\phi_1^n((\phi_1^n)^2 - 1), \\
&\frac{\phi_1^{n+1} - \phi_1^n}{\tau} \\
&= -\sum_{i=1}^{4} \frac{\partial \psi_i^n}{\partial \phi_2^n}\left(\alpha_i + L_i(\mathbf{x}) - \lambda \nabla \cdot \left(\frac{\nabla \psi_i^n}{|\nabla \psi_i^n|}\right)\right) \\
&\quad + 4\sigma\phi_2^n((\phi_2^n)^2 - 1).
\end{aligned} \tag{18}$$

This algorithm is not sensitive to the values of σ and ϵ. We have always used $\sigma = 1$. Some discussions about the value of ϵ will be given later. The algorithm often converges in less than 200 iterations. It is also expected that some other discrete minimization method will accelerate the convergence (Darbon and Sigelle 2006).

3.3 Watersheds and the Piecewise Constant Level Set (PCLS)

The third level set method we propose to use is a new method. It is a variant of the "Piecewise Constant Level Set (PCLS)" method (Lie et al. 2005, 2006b). Piecewise constant level sets have been used for image segmentation in Tai and Yao (2006), Tai et al. (2007), for inverse problems (Tai and Li 2007; Li and Tai 2007a) and for optimal shape design problems (Wei and Wang 2007; Li and Tai 2007b). For this method, only one level set function $\phi : \mathbb{R}^2 \to \mathbb{R}$ is needed, satisfying

$$\kappa(\phi) = (\phi - 1)(\phi - 2)(\phi - 3)(\phi - 4) = 0 \quad \text{in } \Omega, \tag{19}$$

which ensures that ϕ takes piecewise constant values $\phi = \{1, 2, 3, 4\}$. In Tai and Li (2007), Li and Tai (2007a, 2007b), Tai and Yao (2006), Lie et al. (2005 2006b), Christiansen et al. (2006), penalization or Augmented Lagrangian methods were used to deal with the constraint (19). In Jung et al. (2006), it was shown that penalization methods can be connected with Modica-Mortola phase transition model to get even a rigorous convergence analysis.

In this work, we shall use the PCLS method more like a multi-layer level set method of Chung and Vese (2005). Associated with ϕ, we define the characteristic functions for the sub-regions by

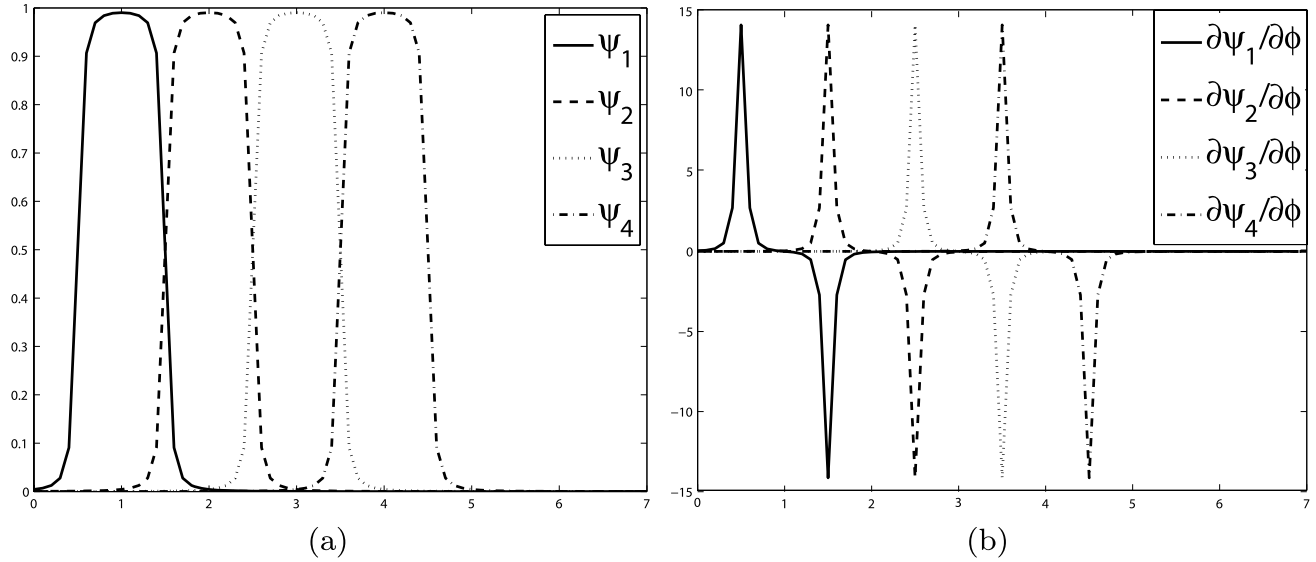

Fig. 3 The characteristic functions ψ_i (**a**) for $\epsilon = 0.005$, $i = \{1, 2, 3, 4\}$ and the corresponding derivatives (**b**). Note how the derivatives are overlapping with their neighbors

$$\psi_i(\phi) = \frac{1}{2}\left(\frac{\phi - i + 0.5}{\sqrt{(\phi - i + 0.5)^2 + \epsilon}} - \frac{\phi - i - 0.5}{\sqrt{(\phi - i - 0.5)^2 + \epsilon}}\right). \tag{20}$$

The first term is an approximation of a step function around $i - 0.5$ and the second term approximates a step function around $i + 0.5$. Figure 3 illustrates the characteristic functions ψ_i for $i = \{1, 2, 3, 4\}$ (a) and their derivatives (b). As noted, the characteristic functions are constructed to ensure that there are overlaps between the support of the derivatives. In order to use this method for the watershed segmentation, we need to solve the following minimization problem:

$$\min_{\phi} \int_\Omega \sum_{i=1}^{4} \{\alpha_i + L_i(\mathbf{x})\}\psi_i(\phi) d\mathbf{x} + \lambda \int_\Omega \sum_{i=1}^{4} |\nabla \psi_i(\phi)| d\mathbf{x} + \gamma \int_\Omega \kappa(\phi)^2 d\mathbf{x}. \tag{21}$$

As in Tai and Li (2007), Li and Tai (2007a, 2007b), Tai and Yao (2006), Lie et al. (2005, 2006b), Christiansen et al. (2006), augmented Lagrangian can be used to solve the above minimization problem. Here, we have just used the penalization method for the constraint $\kappa(\phi) = 0$. Due to the special construction for the characteristic functions ψ_i used in (20), it is not necessary to use large values for the penalization constant γ.

For minimization problem (21), the Euler-Lagrange equation is, c.f. Tai and Chan (2004)

$$\sum_{i=1}^{4} \frac{\partial \psi_i}{\partial \phi}\left(\alpha_i + L_i(\mathbf{x}) - \lambda \nabla \cdot \left(\frac{\nabla \psi_i}{|\nabla \psi_i|}\right)\right) + 2\gamma\kappa \frac{\partial \kappa}{\partial \phi} = 0, \tag{22}$$

where the term $\partial \psi_i / \partial \phi$ is given as

$$\frac{\partial \psi_i}{\partial \phi} = \frac{1}{2}\left(\frac{\epsilon}{((\phi - i + 0.5)^2 + \epsilon)^{\frac{3}{2}}} - \frac{\epsilon}{((\phi - i - 0.5)^2 + \epsilon)^{\frac{3}{2}}}\right). \tag{23}$$

The following explicit gradient flow problem must be solved to steady state:

$$\frac{\phi^{n+1} - \phi^n}{\tau} = -\sum_{i=1}^{4} \frac{\partial \psi_i^n}{\partial \phi^n}\left(\alpha_i + L_i(\mathbf{x}) - \lambda \nabla \cdot \left(\frac{\nabla \psi_i^n}{|\nabla \psi_i^n|}\right)\right) + 2\gamma\kappa^n \frac{\partial \kappa^n}{\partial \phi^n} \tag{24}$$

where $\psi_i^n = \psi_i(\phi^n)$ and $\kappa^n = \kappa(\phi^n)$.

3.4 Differences between the Level Set Methods

We have proposed three different level set methods with different advantages and weak points, producing slightly different results which are complementary to each other. All

three methods produce good results. The Binary level set has several similarities to the Chan-Vese model in the way it produces a fixed number of 2^n phases where n is the number of level set functions. The Piecewise constant level set differs from the Chan-Vese and the Binary level set in several aspects. It only requires a single level set function. Furthermore, it is possible to define the desired number of phases without being limited to a fixed number which is the case for the Chan-Vese model and the Binary level set.

From our numerical experiences, it seems that the Binary level set method is fast and stable for some examples, while the piecewise constant level set method is faster and stable for some other examples. Generally, when the structure of the object is complicated and the number of objects is large, the piecewise constant level set method seems to be advantageous. With three different methods at our disposal, it is an advantage that we can use them to confirm that the obtained results are correct.

4 Numerical Experiments

4.1 Numerical Implementation

All three models have in common the biased topographical distance function, $\alpha_i + L_i(\mathbf{x})$. The values of the topographical distance function inside the markers were approximated by the image values, and α_i was approximated as $\alpha_i \approx \min f(\partial C_i)$, where ∂C_i is the boundary of marker group of color i. The second term $L_i(\mathbf{x})$ was computed as described in Sect. 2.3, one topographical distance function for each group of markers that are inside the same color i. The functions $L_i(\mathbf{x})$ only need to be computed once for the whole computation. The regularization term $\nabla \cdot (\frac{\nabla \psi}{|\nabla \psi|})$ was computed using forward differences (D^+) for the gradient, backward differences (D^-) for the divergence and central differences in the denominator (D),

$$\begin{aligned}
&\nabla \cdot \left(\frac{\nabla \psi_{i,j}^n}{|\nabla \psi_{i,j}^n|} \right) \\
&\quad = D_x^- \left(\frac{D_x^+(\psi_{i,j}^n)}{\sqrt{D_x(\psi_{i,j}^n)^2 + D_y(\psi_{i,j}^n)^2 + \epsilon}} \right) \\
&\qquad + D_y^- \left(\frac{D_y^+(\psi_{i,j}^n)}{\sqrt{D_x(\psi_{i,j}^n)^2 + D_y(\psi_{i,j}^n)^2 + \epsilon}} \right),
\end{aligned} \tag{25}$$

where ϵ is a small parameter to avoid singularities in regions where the gradient is zero. For the Chan-Vese model and the Binary level set, ϕ_1 and ϕ_2 were initialized as zero everywhere which enabled a fast convergence to the correct solution. For the PCLS, it was necessary to initialize the level set function ϕ in a special way, i.e.

$$\phi(\mathbf{x}, t=0) = \begin{cases} 2, & f_{IZ}(\mathbf{x}) \leq 2, \\ 3, & f_{IZ}(\mathbf{x}) \geq 3, \end{cases} \tag{26}$$

where f_{IZ} is the image for the Euclidean influence zones (Sect. 2.5). This initialization increased the computational speed and allowed the level set function to shift freely between the phases.

The watershed lines (watersheds) appear at convergence as the interface between the regions of different colors. To obtain the watersheds, the characteristic functions ψ_i were computed with high accuracy after convergence. For the Chan-Vese model, the exact Heaviside was used in these calculations. For the Binary level set and the PCLS a very small $\epsilon = 10^{-10}$ was used. Then, the characteristic functions ψ_i for all three models were converted into binary functions ψ_i^b by thresholding,

$$\psi_i^b(\mathbf{x}) = \begin{cases} 1, & \psi_i(\mathbf{x}) \geq 0.5, \\ 0, & \psi_i(\mathbf{x}) < 0.5. \end{cases} \tag{27}$$

The outer boundary of the four binary functions $\psi_i^b(\mathbf{x})$ were used as the final watersheds of the image f, $WS(f) = \bigcup_{i=1}^4 \partial \psi_i^b(\mathbf{x})$.

In all experiments values of $\lambda = [0.01, 0.1]$ were chosen for the regularization parameter, depending on the amount of endocytoced particles in the image. A higher amount of noise requires larger λ. The largest possible time-step supporting a stable solution was $\Delta t = 0.1$. A smaller time-step does not change the minimizer in the Chan-Vese model or the Binary level set, but a large number of iterations is required to reach a steady state. For the PCLS, it is critical to use suitable associated settings of Δt, γ and ϵ. Empirically, values of $\Delta t = 0.05$, $\epsilon = 0.1$ and $\gamma = 0.05$ were appropriate as a global setting to converge toward a global minimizer. The same setting for ϵ also applied to the Binary level set. The number of iterations at convergence was between 200 and 400. All numerical code was written in MATLAB®, and the selected images used as examples were processed using one of the three proposed methods in Sects. 3.1–3.3. Additionally a standard marker-controlled watershed segmentation by immersion as implemented in MATLAB® (Vincent and Soille 1991) was calculated for comparison of performance between the two methods. Equal and automatically generated markers were applied to the compared methods in each example.

4.2 Synthetic Data

The level set watershed method was applied to a synthetic image with multiplicative Gaussian noise and a linear gradient to test the robustness of the method. The original image

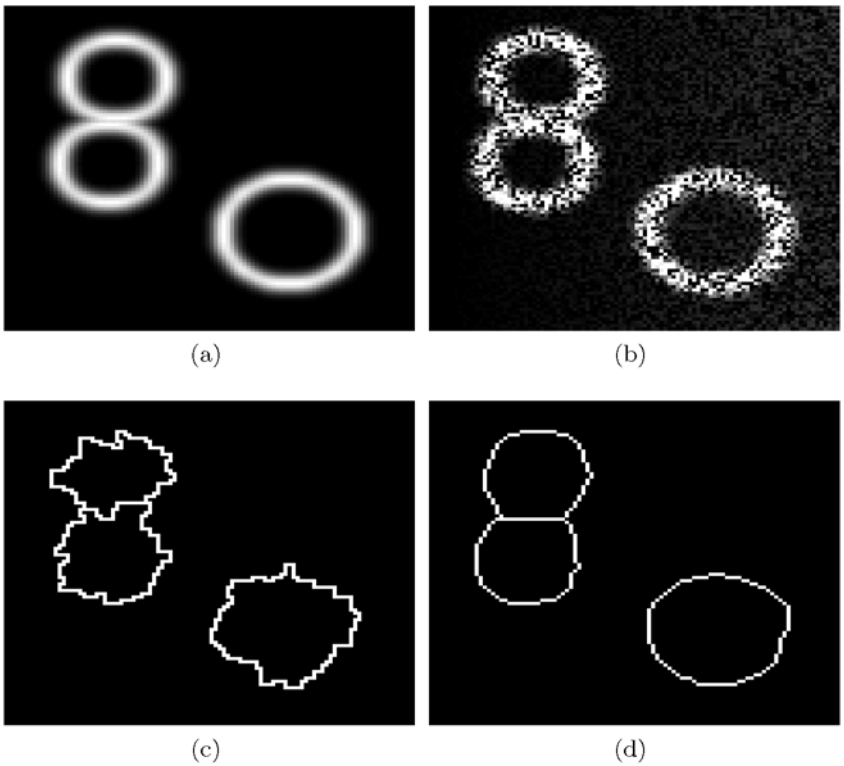

Fig. 4 Segmentation of a synthetic, noisy image. Gaussian multiplicative noise and a linear gradient was added to the original image in (**a**) and the obtained noisy image (**b**) was segmented using the standard watershed (**c**) and the PCLS level set watershed (**d**). Note that the level set watershed has a higher capacity to deal with the noise and the linear gradient than the standard watershed

free from noise is shown in Fig. 4(a), and the same image after addition of Gaussian multiplicative noise and a linear gradient is displayed in (b). The obtained noisy image has a $SNR = 3.4$. The standard watershed segmentation and the PCLS level set watershed segmentation are shown in (c) and (d), respectively. Apparently, the level set watershed has a better ability to deal with the noise.

4.3 Real Data

This section contains experiments involving real cell images taken by fluorescence microscopy showing rat pheochromocytoma PC12 cells (Hodneland et al. 2006). The images are optical planes extracted from 3D stacks. The cells are stained with Wheat Germ Agglutinine (WGA)-Alexa Fluor® which is a lectin that binds glycosylated proteins, thus highlighting the cell membrane. WGA-Alexa Fluor® creates a strong signal from the cell membrane but appears shortly after administration inside the cells due to constitutive endocytosis of the plasma membrane. This causes a significant decrease in the desired signal from the cell membrane and creates correspondingly an increase in undesired signal inside the cell. Figure 5 shows an example of a PC12 cell shortly (a) after administration of WGA-Alexa Fluor® and the same cell one hour later (b). Clearly, the signal from the cell border decreases and simultaneously a brighter signal from internalized vesicles emerges. Endocytosis is the underlying reason for a vast majority of all mis-segmentations in our images, in contrast to the Gaussian noise which represents a minor problem. In this work, we shall use these real images to test the ability of our proposed algorithms.

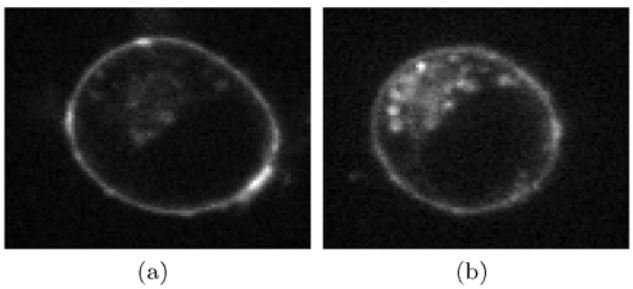

Fig. 5 Endocytosis of WGA. Shortly after administration of WGA-Alexa Fluor® there is a sharp and clear signal from the cell border (**a**). One hour later vesicular structures containing WGA-Alexa Fluor® have been endocytosed, creating a strong signal from inside the cell and at the same time depleting the signal strength from the desired cell border. These processes of endocytosis are responsible for demanding tasks of segmentation

4.4 Convergence in Time, $t \to \infty$

This example contains one cell in addition to background, and it demonstrates the influence of endocytosis on the seg-

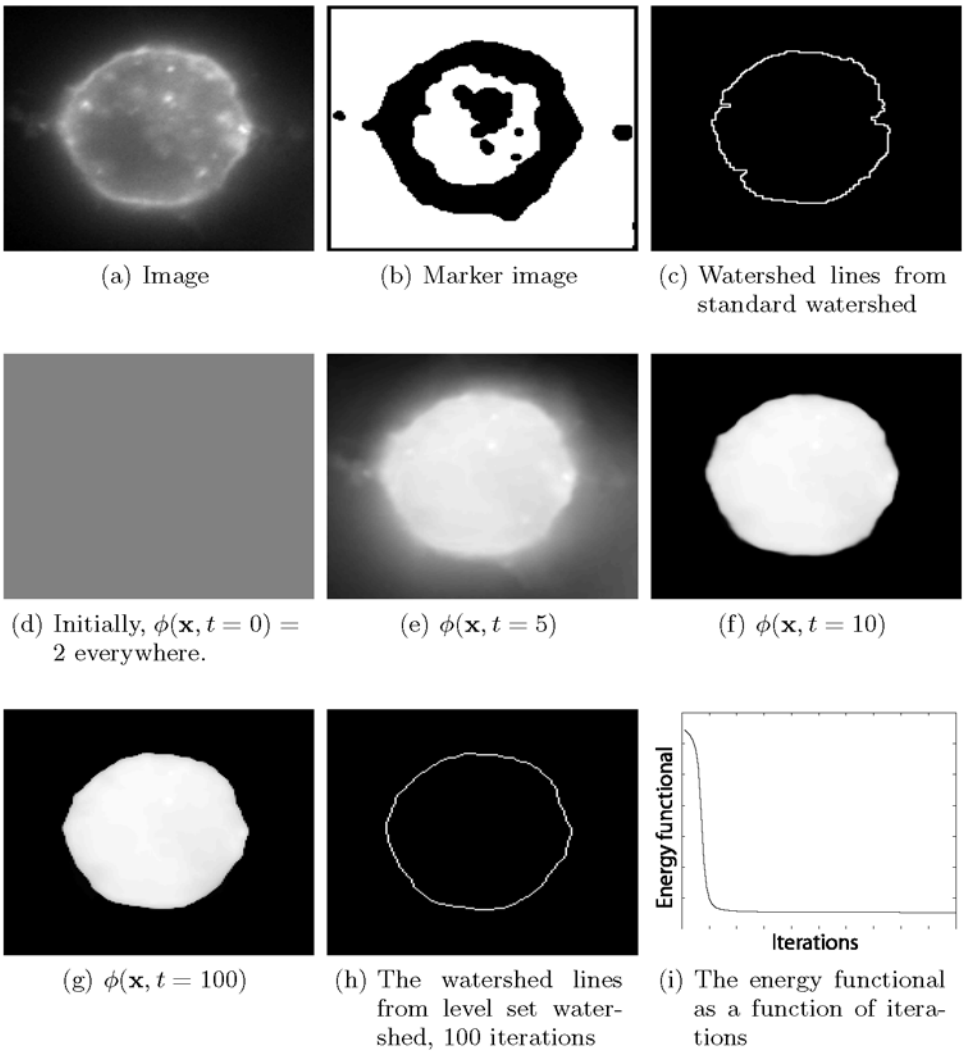

(a) Image (b) Marker image (c) Watershed lines from standard watershed

(d) Initially, $\phi(\mathbf{x}, t = 0) = 2$ everywhere. (e) $\phi(\mathbf{x}, t = 5)$ (f) $\phi(\mathbf{x}, t = 10)$

(g) $\phi(\mathbf{x}, t = 100)$ (h) The watershed lines from level set watershed, 100 iterations (i) The energy functional as a function of iterations

Fig. 6 Watershed segmentation of one cell and a background region. The image in (**a**) was used to create the marker image (**b**) which was used for a standard watershed segmentation (**c**) and a level set watershed segmentation using the Piecewise constant level set (PCLS). The level set function ϕ is shown at different times in (**d**) $t = 0$, (**e**) $t = 5$, (**f**) $t = 20$ and (**g**) $t = 100$, showing that the level set function approaches piecewise constant values. In this case, $\phi \rightarrow \{1 \text{ (dark)}, 2 \text{ (bright)}\}$. The obtained watershed lines from the PCLS are displayed in (**h**), apparently smoother than the watershed lines obtained for the standard watershed (**c**). The panel (**i**) shows the energy functional (21) of the PCLS versus the iterations. The parameter settings for the level set watershed are $\lambda = 0.05$, $\Delta t = 0.1$, $\gamma = 0.1$, $\epsilon = 0.1$

mentation. The image in Fig. 6a was used for segmentation. The method described Sect. 2.2 was used to obtain the marker image (b). The white regions are the markers. Based on the marker image (b), the segmentation using the standard watershed (c) has oscillating boundaries, particularly where the endocytosed particles in the original image are close to the boundary. A segmentation was also performed using the PCLS method. The evolution of the level set function is shown for $t = 0$ (d), $t = 10$ (e), $t = 50$ (f) and $t = 100$ (g). Note that the level set function approaches two piecewise constant regions $\phi \rightarrow \{1 \text{ (dark)}, 2 \text{ (bright)}\}$ at convergence. The interface labels the watershed lines (h). The watershed lines in the level set watershed approach are smoother than in (c). Evidently, this method is more resistant to the influence of endocytosed high intensity particles than the standard watershed. The panel in (i) shows the convergence of the energy functional versus the number of iterations (time t).

4.5 The Regularization Parameter λ

The image in Fig. 7 represents a challenging task of segmentation where the signal from the cell membrane partly disappears or becomes blurry. It shows two attached cells with an inhomogeneously distributed membrane marker, which is the reason for the inhomogeneous signal. The automatically generated marker image in (b) was used for segmentation by the standard watershed (c) and the Piecewise constant level set watershed (PCLS) (d–f). The regularization parameter λ in the level set watershed was given different values (d) $\lambda = 0$, (e) $\lambda = 0.01$ and (f) $\lambda = 0.1$, to demonstrate how λ affects the smoothness of the final watershed lines. Apparently, higher values of λ produce smoother watershed lines, which is to be expected. For a suitably chosen value of λ in (f), the level set watershed segmentation produces smoother boundaries than the standard watershed (c). Generally, a smooth solution is closer to the true boundaries of the cells than an oscillating solution.

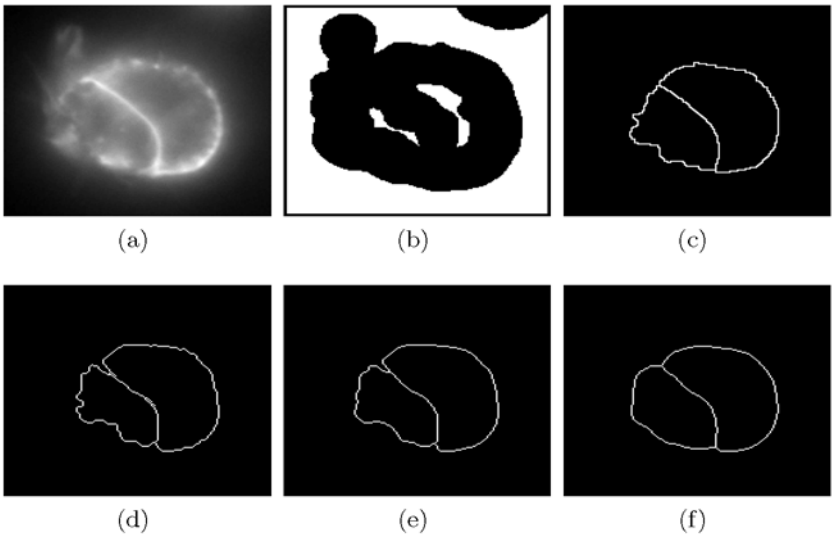

Fig. 7 Watershed segmentation of two cells and a background region. The image in (**a**) was used to automatically obtain the markers in (**b**) using the method of Sect. 2.2. The marker was used for a standard watershed segmentation (**c**) and a level set watershed segmentation (**d–f**). The PCLS watershed segmentation was performed with increasing values of the regularization parameter λ in (**d**) $\lambda = 0$, (**e**) $\lambda = 0.01$ and (**f**) $\lambda = 0.1$ to demonstrate the effect of λ. Note how increasing values of λ create smoother watershed lines. It is also clear that the level set watershed in (**f**) creates smoother watershed lines than the standard watershed in (**c**). This example was created using parameter settings of $\Delta t = 0.1$, $\gamma = 0.1$, $\epsilon = 0.1$, $t = 300$

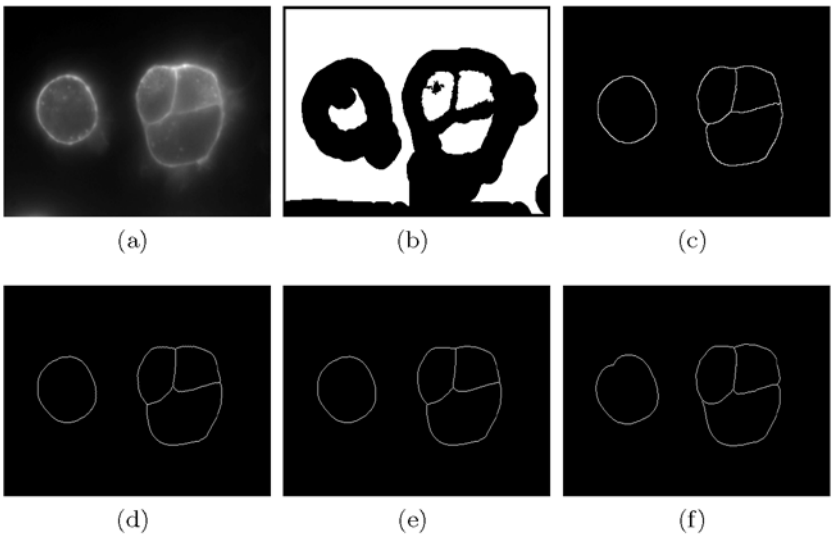

Fig. 8 Watershed segmentation of four cells and a background region. The high-quality image in (**a**) with only weak noise was used to create the marker image (**b**). The marker image was used as input for a standard watershed segmentation (**c**) and for level set watershed segmentation (**d–f**) using the Chan-Vese model (**d**), the Binary level set (**e**) and the PCLS (**f**). Apparently, applied to images of high quality containing weak noise signals, all four models behave very similar. The examples were run with parameter settings of (**d**) $\Delta t = 0.05$, $\lambda = 0.1$, $t = 200$, (**e**) $\Delta t = 0.1$, $\lambda = 0.05$, $\sigma = 0.1$, $t = 200$ and (**f**) $\Delta t = 0.1$, $\lambda = 0.1$, $\gamma = 0.02$, $\epsilon = 0.5$, $t = 300$

4.6 Comparing the Three Level Set Models

The three level set approaches and the standard watershed segmentation produce similar results applied to images with weak noise. This is shown in Fig. 8, where the high-quality image in (a) was used to automatically create the marker image (b). Based on the marker image, a standard watershed segmentation was performed (c) and also the three level set approaches, the Chan-Vese model (d), the Binary level set (e) and the PCLS (f). Evidently, all four models produce very similar segmentation results.

4.7 Regularization Applied to the Level Set Function(s) or the Characteristic Functions

The regularization term enables a smoothing of the watershed lines. This is normally useful for segmentation of real images. However, a smoothing of the watershed lines could also smooth junctions between cells, which is not always appropriate.

In (9), we have used

$$R_1(\phi_1, \phi_2) = \int_\Omega \sum_{i=1}^{4} |\nabla \psi_i| d\mathbf{x}, \tag{28}$$

as the regularization functional. At convergence, $\int_\Omega |\nabla \psi_i| d\mathbf{x}$ is the length of the boundary of region Ω_i. In the original paper (Vese and Chan 2002; Chan and Vese 2001), the regularization functional was different, i.e.

$$R_2(\phi_1, \phi_2) = \int_\Omega \sum_{i=1}^{2} |\nabla \phi_i| d\mathbf{x}. \tag{29}$$

From our numerical experiments, we have observed some interesting phenomena with these two different regularizations. When we increase the regularization parameter λ, we would expect that the watershed lines are getting smoother. This is observed in the experiments, especially see Fig. 9 which is segmented in Fig. 10 for different values of λ and using two different regularization functionals R_1 and R_2. However, the junctions behave differently. For R_2, the corner of the junction in the upper part of the watershed line is getting sharper when the values of λ is getting bigger. While for R_1, the junction is getting smoother when the values of λ is getting bigger. For the PCLS, we can also replace R_1 by

$$R_2(\phi) = \int_\Omega |\nabla \phi| d\mathbf{x}. \tag{30}$$

These two functionals produce different results. In Li and Tai (2007b), it was observed that R_1 can treat triple-junctions in a proper manner. It is known that R_2 given in (29) and (30) are not able to get symmetric triple junctions. Historically, regularization functional R_2 was first proposed in Chan and Vese (2001), while R_1 was first proposed in Lie et al. (2005, 2006a, 2006b).

Oscillating watershed lines are not preferred for segmentation. However, sharp corner may be preferred in some situation. These experiments show that R_1 should be used for these applications.

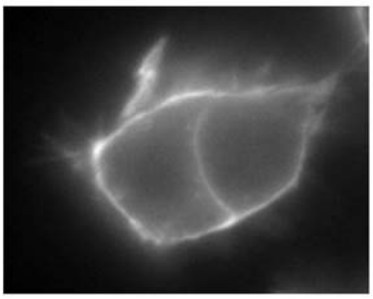

Fig. 9 The image used in Fig. 10 to demonstrate the difference between regularization functionals R_1 and R_2

4.8 Challenging Situations in Real Images

This example shows three PC12 cells with partly inhomogeneously labeled cell membrane. Therefore, it represents a challenging segmentation, approaching the limits of both the standard watershed and the level set watershed segmentation. The image in Fig. 11a was used to create markers automatically (b). The marker image was then applied as input for the standard watershed (c) and also the Binary watershed level set (d–f). The level set functions ϕ_1 and ϕ_2 are displayed in (d) and (e), respectively. The sign of the level set functions is responsible for creating the four phases. The boundaries of the four phases are drawn in (f), showing the final segmentation. Clearly, the watershed level set (f) produces a better segmentation than the standard watershed (c), although none of them is perfect.

4.9 Multiple Objects and the Four-Color Theorem

High-throughput experiments include images of both low and high quality, and any segmentation method should therefore be validated for images of different level of quality. The image in Fig. 12(a) shows one optical plane from an image stack. It represents a severe challenge for segmentation since the boundaries are partly blurred, broken and there exists a significant amount of endocytosed particles. This image also demonstrates the use of the Four-Color coding since this example requires the use of all four colors. The image in Fig. 12(a) was used to automatically construct the marker image Fig. 12(b) which was used as input for the standard watershed segmentation. The obtained watershed lines are shown in Fig. 12(c).

To compute the level set watershed segmentation, the Euclidean influence zones f_{IZ} (Sect. 2.5) were constructed based on the marker image in Fig. 12(b). The Euclidean influence zones were computed with the purpose of grouping the markers in at most four groups according to the Four-Color theorem. The result of this grouping is shown in Fig. 13(a), where all markers are assigned an integer from $1 \rightarrow 4$. The markers possessing the same integer value belong to the same group. Note that all markers within each

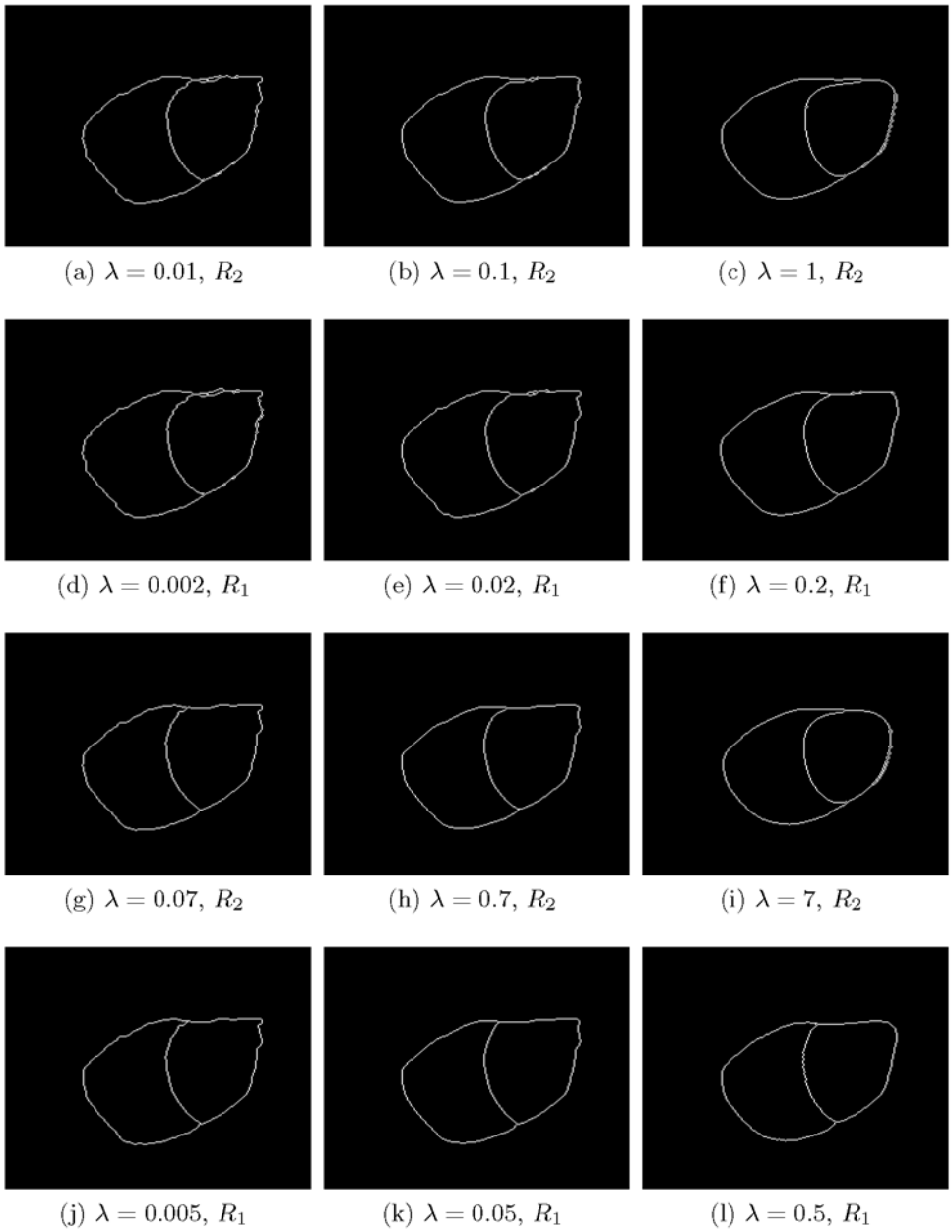

Fig. 10 The difference between regularization functionals R_1 and R_2, demonstrated on the image in Fig. 9. From *left* to *right*, the regularization parameter λ was multiplied by 10. Pictures (**a**–**c**) were created using the Chan-Vese method (see Sect. 3.1) with the regularization functional $R_2(\phi_1, \phi_2)$, and (**d**–**f**) were created using regularization functional $R_1(\phi_1, \phi_2)$. Pictures (**g**–**i**) were computed using the Binary level set (see Sect. 3.2) with the regularization functional $R_2(\phi_1, \phi_2)$ and (**j**–**l**) were created using regularization functional $R_1(\phi_1, \phi_2)$. The right column (largest λ) clearly shows the difference between the regularization functionals. $R_2(\phi_1, \phi_2)$ creates sharper corners with the junctions than the regularization functional $R_1(\phi_1, \phi_2)$. In the test, $\Delta t = 0.005$ for all examples (**a**–**l**)

group are non-adjacent, which is the crucial point. The topographical distance function was calculated around the set of all markers inside each color, and the level set watershed was computed using the Binary level set. The obtained level set functions ϕ_1 and ϕ_2 are shown in Fig. 13(b) and (c), respectively. The two level set functions approach binary values of 0 (black) and 1 (white). The watershed lines from the level set watershed are shown in Fig. 13(d). Note how the level set watershed (Fig. 13(d)) produces smoother watershed lines than the standard watershed (Fig. 12(c)). The level set watershed also captures more of the cells than the standard watershed, selected cells are indicated with asterisks.

4.10 Comparison of Watershed Level Set and Watersnakes

Both the watershed level set and the watersnakes (Nguyen et al. 2003) are algorithms which are able to smooth the watershed lines and they have the topographical distance function in common for their data term. It is therefore to be expected that they produce segmentation results of comparable quality. The image in Fig. 14(a) was used for segmentation by the markers in Fig. 14(b) where one marker is placed inside the cell and another outside the cell indicated as a frame along the image border. For this image, the standard watershed (Fig. 14(c)), the watersnakes (Fig. 14(d)) and the wa-

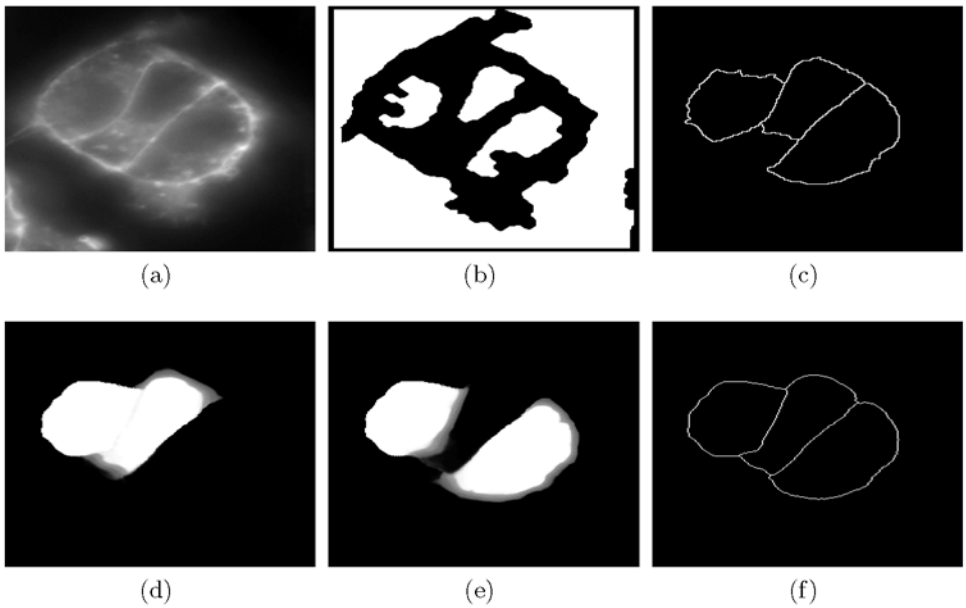

Fig. 11 The image in (**a**) was applied to create markers (**b**) for a standard watershed segmentation (**c**) and also a watershed level set segmentation (**d**–**f**). The four combinations of the sign of the level set functions ϕ_1 (**d**) and ϕ_2 (**e**) settle the boundaries (**f**) of the characteristic functions ψ_i. Note that the level set watershed (**f**) obtains a better segmentation result than the standard watershed (**c**). These examples were executed with parameter settings of $\Delta t = 0.1$, $t = 200$ and $\lambda = 0.1$

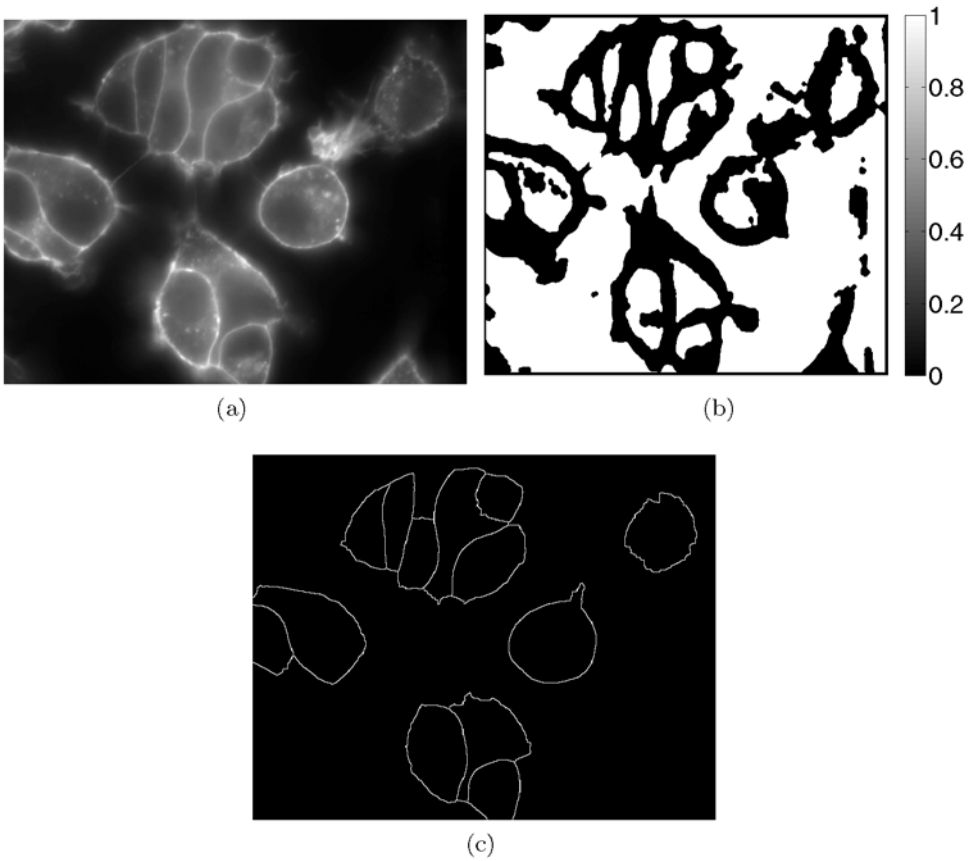

Fig. 12 An optical plane from an image stack (**a**) and the automatically generated binary marker image (**b**) which was used for a standard watershed segmentation (**c**)

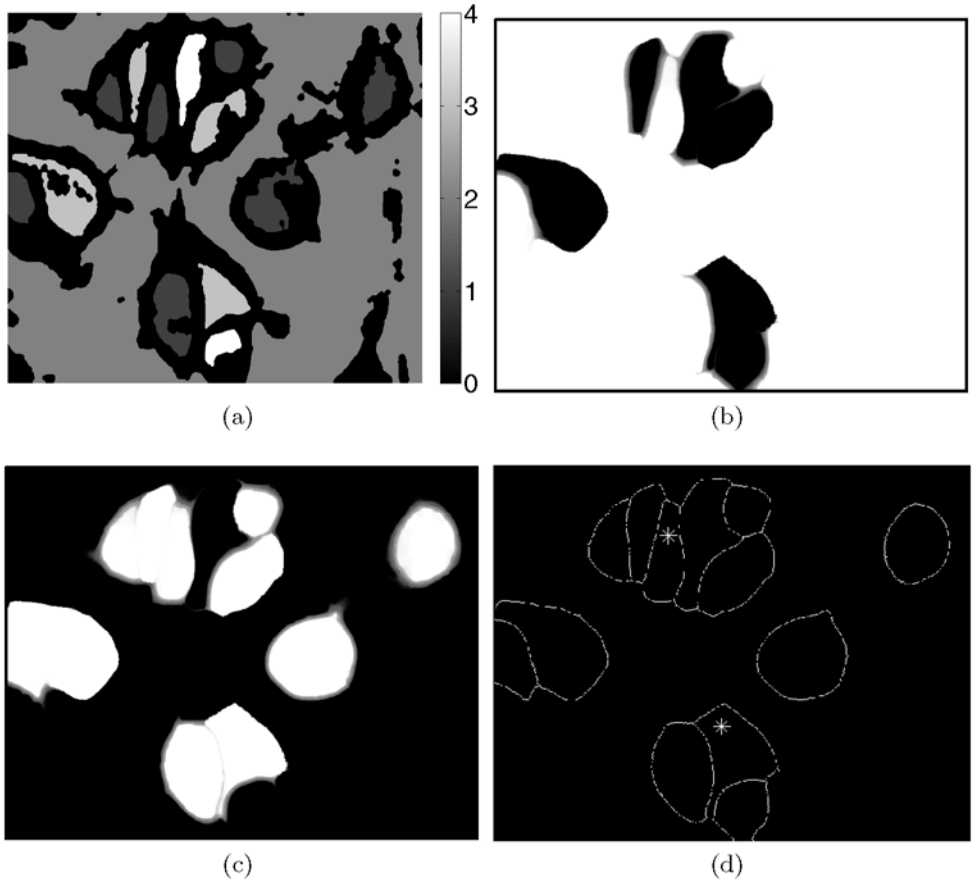

Fig. 13 Segmentation of a high number of cells and demonstration of the Four-Color coding. To compute the level set watershed, the Euclidean influence zones f_{IZ} were calculated around the marker regions in Fig. 12(b), where each region in f_{IZ} represents a specific marker region. The Four-Color theorem was applied to f_{IZ}, grouping the corresponding markers into four groups $\{1, 2, 3, 4\}$, shown in (**a**) where the background has the value zero and all markers belonging to the same group have the same integer value. The Binary level set functions ϕ_1 and $\phi_2 \to \{0, 1\}$ at convergence are displayed in (**b**) and (**c**). The *watershed lines* from the level set watershed are shown in (**d**), producing a smoother result than the standard watershed in Fig. 12(c). The *asterisks* indicate selected cells where the level set watershed captures more of the true cell than the standard watershed. The level set watershed in this example was executed with parameter settings $\Delta t = 0.1, t = 200, \lambda = 0.2, \sigma = 0.01$, and the regularization was applied to the characteristic functions ψ_i

tershed level set (Fig. 14(e)) produce segmentation results of comparable quality. Also for other images comparable segmentation quality was observed between the watersnakes and the watershed level set.

The watersnakes is energy-based and the watershed level set is a variational method and they are thus clearly distinguishable. Due to their different formulation and at the same time comparable performance they can therefore be regarded as complementary algorithms. However, the watershed level set is expected to be faster than the watersnakes in situations involving a large number of objects since the watershed level set requires the computation of maximum four topographical distance functions regardless of the number of objects. For a small number of objects the watersnakes are probably faster than the watershed level set since the latter is an iterative method. Within the variational framework the watershed level set can be easily augmented with additional features by adding new terms into the cost functional. This is probably also possible for the watersnakes, but it has not been demonstrated so far. For example, one could penalize watershed regions with holes, watershed regions deviating from pre-defined shapes or those of convex shape. To demonstrate the flexibility of the watershed level set, we have here added a term controlling the size of the watershed regions by penalizing regions below a certain threshold. Such a term can be useful to expunge superfluous watershed regions in over-segmentation. We choose the Binary level set approach and therefore consider the energy functional in (15). Note that the area of every characteristic function ψ_i equals $y_i = \int_\Omega \psi_i d\mathbf{x}$. Minimizing the functional

$$G(\phi_1, \phi_2) = F(\phi_1, \phi_2) + \eta \sum_i f(y_i) \tag{31}$$

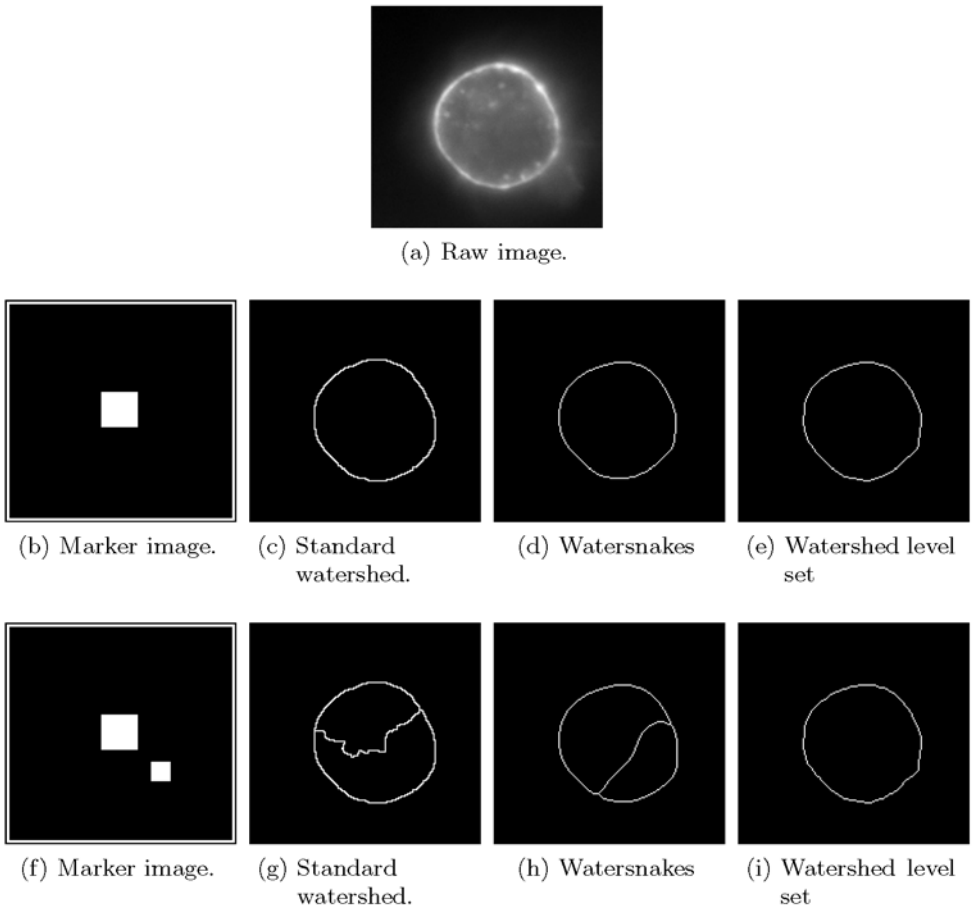

Fig. 14 Comparing standard watershed, watersnakes and watershed level set. The image in (**a**) was used for segmentation. In (**b**–**f**), two correctly placed markers (**b**) produce comparable segmentation results for standard watershed (**c**), watersnakes (**d**) and watershed level set (**d**). However, in (**f**) an additional marker has been added to the cell, a situation naturally occurring in automated marker construction. In this case, the standard watershed (**g**) and the watersnakes (**h**) create an over-segmentation but the watershed level set based on (33) is able to combine the segmentation with a merging which correctly expunges either one of the superfluous watershed regions

will therefore penalize watershed regions with area less than A where f is a decreasing function from 1 to 0,

$$f(y_i) = \frac{1}{2}\left(1 - \frac{y_i - A}{\sqrt{(y_i - A)^2 + \epsilon}}\right) \quad \text{and}$$
$$f'(y_i) = -\frac{\epsilon}{2((y_i - A)^2 + \epsilon)^{3/2}}. \tag{32}$$

η is a weighting parameter in (31). The Euler-Lagrange equations obtained for this minimization is

$$\sum_{i=1}^{4} \frac{\partial \psi_i}{\partial \phi_1}\left(\alpha_i + L_i(\mathbf{x}) - \lambda\nabla\cdot\left(\frac{\nabla\psi_i}{|\nabla\psi_i|}\right) + \eta f'(y_i)\right) + 4\sigma\phi_1(\phi_1^2 - 1) = 0,$$
$$\sum_{i=1}^{4} \frac{\partial \psi_i}{\partial \phi_2}\left(\alpha_i + L_i(\mathbf{x}) - \lambda\nabla\cdot\left(\frac{\nabla\psi_i}{|\nabla\psi_i|}\right) + \eta f'(y_i)\right) + 4\sigma\phi_2(\phi_2^2 - 1) = 0, \tag{33}$$

where ϵ controls the smoothness of f and can be set globally for a given set of images. The effect of (31) is demonstrated in Fig. 14 where the image in (a) was used for segmentation in conjunction with the marker image (f) which contains two markers for the given cell. The standard watershed (g) and the watersnakes (h) create an expected over-segmentation. However, the watershed level set is capable of expunging one of the superfluous watershed regions and thus simultaneously performing a segmentation and a merging.

5 Conclusion

In this work we have combined the level set method (Osher and Sethian 1988; Vese and Chan 2002; Chan and Vese 2001; Lie et al. 2005, 2006a, 2006b) and the marker-controlled watershed segmentation (Najman and Schmitt 1994; Meyer 1994; Vincent and Dougherty 1994; Vincent and Soille 1991) to develop a method for segmentation of real cells and other structures of similar nature. A set of markers, also called initialization regions, were automatically created by adaptive thresholding and iterative filling (Sect. 2.2). Such automated methods are of high value in high-throughput experiments and other experimental setups producing large amount of data. Based on the markers, the watershed distance transform was computed from the topographical distance function (Meyer 1994). We then used the Four-Color theorem to group the markers into a maximum

of four groups, thus reducing the complexity of the problem. Inspired by Nguyen et al. (2003), we propose to compute the watershed lines around each group of markers using three different level set approaches, Sects. 3.1–3.3. These level set methods were tested for real and synthetic images of different complexity, and containing a large number of cells. The experimental results show that all three level set methods are able to perform a good segmentation of the given images with comparable performance to the standard watershed and the watersnakes.

References

Adiga, P. S. U. (2003). Integrated approach for segmentation of 3-D confocal images of a tissue specimen. *Microscopy Research and Technique*, *54*(4), 260–270.

Adiga, P. S. U., & Chaudhuri, B. B. (1999). Efficient cell segmentation tool for confocal microscopy tissue images and quantitative evaluation of fish signals. *Microscopy Research and Technique*, *44*(1), 49–68.

Adiga, U., Malladi, R., Fernandez-Gonzalez, R., & Ortiz de Solorzano, C. (2006). High-throughput analysis of multispectral images of breast cancer tissue. *IEEE Transactions on Image Processing*, *15*(8), 2259–2268.

Appel, K. I., & Haken, W. (1977). Every planar map is four colorable. *Illinois Journal of Mathematics*, *21*, 429–567.

Arbeléz, P. A., & Cohen, L. D. (2004). Energy partitions and image segmentation. *Journal of Mathematical Imaging and Vision*, *20*(1–2), 43–57.

Baggett, D., Nakaya, M., McAuliffe, M., Yamaguchi, T. P., & Lockett, S. (2005). Whole cell segmentation in solid tissue sections. *Cytometry Part A*, *67A*, 137–143.

Bamford, P., & Lovell, B. (1998). Unsupervised cell nucleus segmentation with active contours. *Signal Processing*, *71*(2), 203–213.

Bengtsson, E., Wählby, C., & Lindblad, J. (2004). Robust cell image segmentation methods. *Pattern Recognition and Image Analysis*, *14*, 157–167.

Caselles, V., Catté, F., Coll, T., & Dibos, F. (1993). A geometric model for active contours in image processing. *Numerical Mathematics*, *66*(1), 1–31.

Chambolle, A. (2004). An algorithm for total variation minimization and applications. *Journal of Mathematical Imaging and Vision*, *20*(1–2), 89–97. Special issue on mathematics and image analysis.

Chan, T., & Vese, L. (2001). Active contours without edges. *IEEE Transactions on Image Processing*, *10*, 266–277.

Chan, T. F., Moelich, M., & Sandberg, B. (2006). Some recent developments in variational image segmentation. In X.-C. Tai, K. A. Lie, T. Chan & S. Osher (Eds.), *Image processing based on partial differential equations* (pp. 175–201). Heidelberg: Springer.

Chan, T. F., & Tai, X.-C. (2004). Level set and total variation regularization for elliptic inverse problems with discontinuous coefficients. *Journal of Computational Physics*, *193*(1), 40–66.

Chang, S. G., Yu, B., & Vetterli, M. (2000). Spatially adaptive wavelet thresholding with context modeling for image denoising. *IEEE Transactions on Image Processing*, *9*(9), 1522–1531.

Chien, S. Y., Huang, Y. W., & Chen, L. G. (2003). Predictive watershed: a fast watershed algorithm for video segmentation. *CirSysVideo*, *13*(5), 453–461.

Christiansen, O., & Tai, X.-C. (2006). Fast implementation of piecewise constant level set methods. In X.-C. Tai, K. A. Lie, T. Chan & S. Osher (Eds.), *Image processing based on partial differential equations* (pp. 289–308). Heidelberg: Springer.

Chung, G., & Vese, L. A. (2005). Energy minimization based segmentation and denoising using a multilayer level set approach. In *Energy minimization methods in computer vision and pattern recognition* (Vol. 3757, pp. 439–455). Heidelberg: Springer.

Cremers, D., Tischhäuser, F., Weickert, J., & Schnörr, C. (2002). Diffusion snakes: introducing statistical shape knowledge into the Mumford–Shah functional. *International Journal of Computer Vision*, *50*, 295–313.

Darbon, J., & Sigelle, M. (2006). Image restoration with discrete constrained total variation. I. Fast and exact optimization. *Journal of Mathematical Imaging and Vision*, *26*(3), 261–276.

Dow, A. I., Shafer, S. A., Kirkwood, J. M., Mascari, R. A., & Waggoner, A. S. (1996). Automatic multiparameter fluorescence imaging for determining lymphocyte phenotype and activation status in melanoma tissue sections. *Cytometry*, *25*, 71–81.

Dufour, A., Shinin, V., Tajbakhsh, S., Guillen-Aghion, N., Olivo-Marin, J.-C., & Zimmer, C. (2005). Segmenting and tracking fluorescent cells in dynamic 3-d microscopy with coupled active surfaces. *IEEE Transactions on Image Processing*, *14*(9), 1396–1410.

Felkel, P., Bruckschwaiger, M., & Wegenkittl, R. (2002). Implementation and complexity of the watershed-from-markers algorithm computed as a minimal cost forest. *Computer Graphics Forum*, *20*, 2001.

Fok, Y.-L., Chan, J. C. K., & Chin, R. T. (1996). Automated analysis of nerve-cell images using active contour models. *IEEE Transactions on Medical Imaging*, *15*(3).

Gautama, S., Goeman, W., & D'Haeyer, J. (2004). Robust detection of road junctions in vhr images using an improved ridge detector. *The International Archives of Photogrammetry, Remote Sensing and Spatial Information Sciences, 34*.

Gebhard, M., Mattes, J., & Eils, R. (2001). An active contour model for segmentation based on cubic b-splines and gradient vector flow. In *MICCAI '01: Proceedings of the 4th international conference on medical image computing and computer-assisted intervention*, London, UK, 2001 (pp. 1373–1375). Berlin: Springer.

Gonzalez, R. C., & Woods, R. E. (1992). *Digital image processing*. Reading: Addison-Wesley.

Grau, V., Mewes, A. J. U., Alca-iz Raya, M., Kikinis, R., & Warfield, S. K. (2004). Improved watershed transform for medical image segmentation using prior information. *IEEE Transactions on Medical Imaging*, *23*(4), 447–458.

Jung, Y. M., Kang, S. H., & Shen, J. (2006). Multiphase image segmentation via modica-mortola phase transition. *SIAM Journal on Applied Mathematics*, *67*(5), 1213–1232.

Hodneland, E., Lundervold, A., Gurke, S., Tai, X.-C., Rustom, A., & Gerdes, H.-H. (2006). Automated detection of tunneling nanotubes in 3d images. *Cytometry Part A*, *69A*, 961–972.

Kass, M., Witkin, A., & Terzopoulos, D. (1988). Snakes: Active contour models. *International Journal of Computer Vision*, *V1*(4), 321–331.

Li, H., & Tai, X.-C. (2007a). Piecewise constant level set method for interface problems. In *Internat. ser. numer. math.: Vol. 154. Free boundary problems* (pp. 307–316). Basel: Birkhäuser.

Li, H., & Tai, X.-C. (2007b). Piecewise constant level set method for multiphase motion. *International Journal of Numerical Analysis and Modeling*, *4*(2), 291–305.

Lie, J., Lysaker, M., & Tai, X.-C. (2005). A piecewise constant level set framework. *International Journal of Numerical Analysis and Modeling*, *2*(4), 422–438.

Lie, J., Lysaker, M., & Tai, X.-C. (2006a). A binary level set model and some applications to Mumford-Shah image segmentation. *IEEE Transactions on Image Processing*, *15*(5), 1171–1181.

Lie, J., Lysaker, M., & Tai, X.-C. (2006b). A variant of the level set method and applications to image segmentation. *Mathematics of Computation*, *75*(255), 1155–1174.

Lindblad, L. (2002). *Development of algorithms for digital image cytometry*. Ph.D. thesis. Acta Universitatis Upsaliensis, 2002.

Lu, T., Neittaanmäki, P., & Tai, X.-C. (1991). A parallel splitting up method and its application to Navier-Stokes equations. *Applied Mathematics Letters*, *4*(2), 25–29.

Lu, T., Neittaanmäki, P., & Tai, X.-C. (1992). A parallel splitting-up method for partial differential equations and its applications to Navier-Stokes equations. *RAIRO Modélisation Mathématique et Analyse Numérique*, *26*(6), 673–708.

Malpica, N., Ortiz de Solórzano, C., Vaquero, J. J., Santos, A., Vallcorba, I., Garcia-Sagredo, J. M., & Francisco del, P. (1997). Applying watershed algorithms to the segmentation of clustered nuclei. *Cytometry*, *28*, 289–297.

Meyer, F. (1994). Topographic distance and watershed lines. *Signal Processing*, *38*(1), 113–125.

Mumford, D., & Shah, J. (1989). Optimal approximation by piecewise smooth functions and associated variational problems. *Communications on Pure Applied Mathematics*, *42*, 577–685.

Najman, L., & Schmitt, M. (1994). Watershed of a continuous function. *Signal Processing*, *38*(1), 99–112.

Nath, S. K., Palaniappan, K., & Bunyak, F. (2006). Cell segmentation using coupled level sets and graph-vertex coloring. In *MICCAI (1)* (pp. 101–108).

Nguyen, H. T., Worring, M., & van den Boomgaard, R. (2003). Watersnakes: Energy-driven watershed segmentation. *IEEE Transactions on PAMI*, *25*(3), 330–342.

Nielsen, L. K., Tai, X.-C., Aanonsen, S. I., & Espedal, M. (2006). Reservoir description using a binary level set model. In X.-C. Tai, K. A. Lie, T. Chan & S. Osher (Eds.), *Image processing based on partial differential equations* (pp. 403–426). Heidelberg: Springer.

Nielsen, L. K., Tai, X.-C., Aanonsen, S. I., & Espedal, M. (2007). A binary level set model for elliptic inverse problems with discontinuous coefficients. *International Journal of Numerical Analysis and Modeling*, *4*(1), 74–99.

Osher, S., & Sethian, J. A. (1988). Fronts propagating with curvature-dependent speed: Algorithms based on Hamilton-Jacobi formulations. *Journal of Computational Physics*, *79*, 12–49.

Osma-Ruiz, V., Godino-Llorente, J. I., Sáenz-Lechón, N., & Gómez-Vilda, P. (2007). An improved watershed algorithm based on efficient computation of shortest paths. *Pattern Recognition*, *40*(3), 1078–1090.

Rambabu, C., & Chakrabarti, I. (2007). An efficient immersion-based watershed transform method and its prototype architecture. *Journal of Systems Architecture*, *53*(4), 210–226.

Robertson, N., Sanders, D., Seymour, P., & Thomas, R. (1996). A new proof of the four colour theorem. *Electronic Research Announcements of the American Mathematical Society*, *2*(1), 17–25.

Roerdink, J., & Meijster, A. (1999). *The watershed transform: Definitions, algorithms and parallelization strategies*. Institute for Mathematics and Computer Science, University of Groningen, Groningen, The Netherlands, IWI 99–9-06.

Ortiz De Solorzano, C., Malladi, R., Lelièvre, S. A., & Lockett, S. J. (2001). Segmentation of nuclei and cells using membrane related protein markers. *Journal of Microscopy*, *201*, 404–415.

Song, B., & Chan, T. (2002). *Fast algorithm for level set based optimization* (UCLA CAM Report, CAM-02-68).

Tai, X.-C., & Chan, T. F. (2004). A survey on multiple level set methods with applications for identifying piecewise constant functions. *International Journal of Numerical Analysis and Modeling*, *1*(1), 25–47.

Tai, X.-C., Hodneland, E., Weickert, J., Buroresthliev, N. V., Lundervold, A., & Gerdes, H.-H. (2007). Level set methods for watershed image segmentation. In *LNCS: Vol. 4485. Scale space and variational methods in computer vision* (pp. 178–190). Berlin: Springer.

Tai, X.-C., & Li, H. (2007). A piecewise constant level set method for elliptic inverse problems. *Applied Numerical Mathematics*, *57*(5–7), 686–696.

Tai, X.-C., & Yao, C.-H. (2006). Image segmentation by piecewise constant Mumford-Shah model without estimating the constants. *Journal of Computational Mathematics*, *24*(3), 435–443.

Vese, L. A., & Chan, T. F. (2002). A multiphase level set framework for image segmentation using the Mumford and Shah model. *International Journal of Computer Vision*, *50*(3), 271–293.

Vincent, L., & Dougherty, E. R. (1994). Morphological segmentation for textures and particles. In E. Dougherty (Ed.), *Digital image processing methods* (pp. 43–102). New York: Dekker.

Vincent, L., & Soille, P. (1991). Watersheds in digital spaces: An efficient algorithm based on immersion simulations. *IEEE Transactions on Pattern Analysis and Machine Intelligence*, *13*(6), 583–598.

Wählby, C., Sintorn, I.-M., Erlandsson, F., Borgefors, G., & Bengtsson, E. (2004). Combining intensity, edge and shape information for 2d and 3d segmentation of cell nuclei in tissue sections. *Journal of Microscopy*, *215*, 67–76.

Wei, P., & Wang, M. Y. (2007). A piecewise constant level set method for structural shape and topology optimization. In *7th World congress of structural and multidisciplinary optimization, Seoul, Korea*, 2007.

Weickert, J., Romeny, B., & Viergever, M. (1998). Efficient and reliable schemes for nonlinear diffusion filtering. *IEEE Transactions on Image Processing*, *7*(3), 398–410.

Xu, C., & Prince, J. (1998). Snakes, shapes, and gradient vector flow. *IEEE Transactions on Image Processing*, *7*(3), 359–369.